

*Digital Comprehensive Summaries of Uppsala Dissertations  
from the Faculty of Medicine 1968*

# Identification of protease inhibitors against Flaviviruses and Coronaviruses

DARIO AKABERI



ACTA UNIVERSITATIS  
UPSALIENSIS  
2023

ISSN 1651-6206  
ISBN 978-91-513-1872-1  
urn:nbn:se:uu:diva-508907



UPPSALA  
UNIVERSITET

Dissertation presented at Uppsala University to be publicly examined in Lecture hall IX, Uppsala University main building, Biskopsgatan 3 753 10 Uppsala, Uppsala, Thursday, 28 September 2023 at 13:00 for the degree of Doctor of Philosophy (Faculty of Medicine). The examination will be conducted in English. Faculty examiner: Associate Professor Ujjwal Neogi (Department of Laboratory Medicine, clinical microbiology, Karolinska Institute).

### Abstract

Akaberi, D. 2023. Identification of protease inhibitors against Flaviviruses and Coronaviruses. *Digital Comprehensive Summaries of Uppsala Dissertations from the Faculty of Medicine* 1968. 68 pp. Uppsala: Acta Universitatis Upsaliensis. ISBN 978-91-513-1872-1.

Vector-borne flaviviruses and coronaviruses of zoonotic origins are important human pathogens and represent a serious threat to public health worldwide. Flaviviruses can be found on all continents, apart from Antarctica, where they are transmitted by arthropod vectors causing millions of infections every year. While most of the infections are mild or asymptomatic, flaviviruses like dengue and yellow fever viruses can cause potentially lethal hemorrhagic fever and shock syndrome. Neurotropic flaviviruses like West Nile, Japanese encephalitis, and Tick-borne encephalitis (TBEV) can cause meningoencephalitis with long-term symptoms.

Coronaviruses, and in particular betacoronaviruses of zoonotic origin like SARS (2003) and MERS (2012), have been periodically emerging since the early 2000s causing outbreaks of severe respiratory syndrome. The latest example is SARS-CoV-2 that after causing a cluster of infection in the Chinese city of Wuhan, spread all over the world causing at present over 6.9 million deaths. Although vaccines are essential in preventing infections or severe disease and hospitalization in the case of SARS-CoV-2, antivirals represent an extremely valuable tool for treatment and prevention of current and future flavivirus and coronavirus infections. In the work presented in this thesis we have used a combination of in silico and in vitro techniques to identify and test the activity of potential inhibitors of viral proteases.

In our first study (paper 1) we unexpectedly identified an HIV protease inhibitor with in vitro activity against ZIKV NS2B-NS3 protease. The inhibitor was identified by virtual screening of a library of known protease inhibitors, evaluated by molecular dynamics simulation and finally tested against recombinant ZIKV protease using a FRET-based enzymatic assay. The same combination of molecular docking and molecular dynamics simulations were also used to correctly predict the activity of a known pan-Flavivirus protease inhibitor against TBEV protease (paper 2). As a result, we were the first to report peptide-based compounds with in vitro activity against TBEV.

After the outbreak of the COVID-19 we switched our attention to SARS-CoV-2. We first tested the inhibitory effect of the broad-spectrum antiviral nitric oxide (NO) and found that the NO-releasing compound SNAP had a dose dependent inhibitory effect on SARS-CoV-2 replication in cell-based assays (paper 3). We speculated that SNAP could inhibit SARS-CoV-2 protease by trans-nitration of the catalytic Cys145 of SARS-CoV-2 main protease and found that SNAP had a dose dependent inhibitory effect on recombinant SARS-CoV-2 Mpro protease activity in an in vitro enzymatic assay. In our last study (paper 4) we identified a new class of potent SARS-CoV-2 protease inhibitors through the affinity screening of DNA-encoded-chemical libraries containing 4.2 billion compounds. The identified compounds inhibited recombinant SARS-CoV-2 protease with IC<sub>50</sub> as low as 25 nM and had a dose dependent antiviral effect in the low micromolar range in infected Calu-3 and Caco-2 cell lines.

**Keywords:** Antiviral research, protease inhibitors, flaviviruses, coronaviruses, ZIKV, TBEV, SARS-CoV-2

*Dario Akaberi, Department of Medical Sciences, Clinical Microbiology, Akademiska sjukhuset, Uppsala University, SE-751 85 Uppsala, Sweden. Department of Medical Biochemistry and Microbiology, Box 582, Uppsala University, SE-75123 Uppsala, Sweden.*

© Dario Akaberi 2023

ISSN 1651-6206

ISBN 978-91-513-1872-1

URN urn:nbn:se:uu:diva-508907 (<http://urn.kb.se/resolve?urn=urn:nbn:se:uu:diva-508907>)

*To my nephew*

*“I asked the question for the best reason possible, for the only reason, indeed, that excuses anyone for asking any question - simple curiosity.”*

*Oscar Wilde*



# List of Papers

This thesis is based on the following papers, which are referred to in the text by their Roman numerals.

- I. **Akaberi, D.**, Chinthakindi, P.K., Båhlström, A., Palanisamy, N., Sandström, A., Lundkvist, Å., Lennerstrand, J. (2020) Identification of a C2-symmetric diol based human immunodeficiency virus protease inhibitor targeting Zika virus NS2B-NS3 protease. *Journal of Biomolecular Structure and Dynamics*, 38(18): 5526–5536.
- II. **Akaberi, D.**, Båhlström, A., Chinthakindi, P.K., Nyman, T., Sandström, A., Järhult, J.D., Palanisamy, N., Lundkvist, Å., Lennerstrand, J. (2021) Targeting the NS2B-NS3 protease of tick-borne encephalitis virus with pan-flaviviral protease inhibitors. *Antiviral Research*, 190, 105074
- III. **Akaberi, D.**, Krambrich, J., Ling, J., Luni, C., Hedenstierna, G., Järhult, J.D., Lennerstrand, J., Lundkvist, Å. (2020) Mitigation of the replication of SARS-CoV-2 by nitric oxide in vitro. *Redox Biology*, 37, 101734.
- IV. **Akaberi, D.**, Lati, P.M., Krambrich, J., Berger, J., Turunen, P., Gullberg, H., Moche, M., Chinthakindi, K.P., Nyman, T., Sandström, A., Järhult, J.D., Sandberg, K., Lundkvist, Å., Verho, O., Lennerstrand, J. (manuscript in preparation).

Reprints were made with permission from the respective publishers.

## Additional publications, not included in the thesis

- I. Palanisamy, N., **Akaberi, D.**, Lennerstrand, J. (2018) Protein backbone flexibility pattern is evolutionarily conserved in the Flaviviridae family: A case of NS3 protease in Flavivirus and Hepacivirus. *Molecular Phylogenetics and Evolution*, 118:58–63.
- II. **Akaberi, D.**, Bergfors, A., Kjellin, M., Kameli, N., Lidemalm, L., Kolli, B., Shafer, R.W., Palanisamy, N., Lennerstrand, J. (2018) Baseline dasabuvir resistance in Hepatitis C virus from the genotypes 1, 2 and 3 and modeling of the NS5B-dasabuvir complex by the in silico approach. *Infection Ecology & Epidemiology*, 8(1), 1528117
- III. Palanisamy, N., **Akaberi, D.**, Lennerstrand, J., Lundkvist, Å. (2018) Comparative genome analysis of Alkhumra hemorrhagic fever virus with Kyasanur forest disease and tick-borne encephalitis viruses by the in silico approach. *Pathogens and Global Health*, 112(4):210–226.
- IV. Kileng, H., Kjellin, M., **Akaberi, D.**, Bergfors, A., Duberg, A.-S., Wesslén, L., Danielsson, A., Gangsøy Kristiansen, M., Gutteberg, T., Goll, R., Lannergård, A., Lennerstrand, J. (2018) Personalized treatment of hepatitis C genotype 1a in Norway and Sweden 2014-2016: a study of treatment outcome in patients with or without resistance-based DAA-therapy. *Scandinavian Journal of Gastroenterology*, 53(10-11):1347–1353.
- V. Palanisamy, N., Kalaghatgi, P., **Akaberi, D.**, Lundkvist, Å., Chen, Z.-W., Hu, P., Lennerstrand, J. (2018) Worldwide prevalence of baseline resistance-associated polymorphisms and resistance mutations in HCV against current direct-acting antivirals. *Antiviral Therapy*, 23(6):485–493.

- VI. Kjellin, M., Kileng, H., **Akaberi, D.**, Palanisamy, N., Duberg, A.-S., Danielsson, A., Kristiansen, M.G., Nöjd, J., Aleman, S., Gutteberg, T. (2019) Effect of the baseline Y93H resistance-associated substitution in HCV genotype 3 for direct-acting antiviral treatment: real-life experience from a multicenter study in Sweden and Norway. *Scandinavian journal of gastroenterology*, 54(8):1042–1050.
- VII. Nissen, K., Krambrich, J., **Akaberi, D.**, Hoffman, T., Ling, J., Lundkvist, Å., Svensson, L., Salaneck, E. (2020) Long-distance airborne dispersal of SARS-CoV-2 in COVID-19 wards. *Scientific Reports*, 10(1), 19589
- VIII. Nissen, K., Hagbom, M., Krambrich, J., **Akaberi, D.**, Sharma, S., Ling, J., Hoffman, T., Lundkvist, Å., Svensson, L., Bondeson, K., Salaneck, E. (2021) Presymptomatic viral shedding and infective ability of SARS-CoV-2; a case report. *Heliyon* 7(2), e06328.
- IX. Krambrich, J., **Akaberi, D.**, Ling, J., Hoffman, T., Svensson, L., Hagbom, M., Lundkvist, Å. (2021) SARS-CoV-2 in hospital indoor environments is predominantly non-infectious. *Virology Journal* 18(1):1-9.
- X. Luttens, A., Gullberg, H.,<sup>‡</sup> Abdurakhmanov, E.,<sup>‡</sup> Vo, D.D.,<sup>‡</sup> **Akaberi, D.**,<sup>‡</sup> Talibov, V.O., Nekhotiaeva, N., Vangeel, L., De Jonghe, S., Jochmans, D., Krambrich, J., Tas, A., Lundgren, B., Gravenfors, Y., Craig, A.J., Atilaw, Y., Sandström, A., Moodie, L.W.K., Lundkvist, Å., van Hemert, M.J., Neyts, J., Lennerstrand, J., Kihlberg, J., Sandberg, K., Danielson, U.H., Carlsson, J. (2022) Ultralarge Virtual Screening Identifies SARS-CoV-2 Main Protease Inhibitors with Broad-Spectrum Activity against Coronaviruses. *Journal of the American Chemical Society*, 144(7):2905–2920.
- XI. Hoffman, T., Kolstad, L., **Akaberi, D.**, Järhult, J.D., Rönnerberg, B., Lundkvist, Å. (2023) Reduced Binding between Omicron B. 1.1. 529 and the Human ACE2 Receptor in a Surrogate Virus Neutralization Test for SARS-CoV-2. *Viruses*, 15(6), 1280.

<sup>‡</sup>Equal contribution





# Contents

Introduction.....	13
The flavivirus genus .....	14
Classification, structure, and genome organization: .....	14
Life cycle: .....	14
Flaviviruses epidemiology and disease: .....	16
Zika virus.....	18
Tick-borne encephalitis virus .....	19
Flavivirus protease as target for the development of antivirals.....	20
SARS-CoV-2.....	22
Classification, structure, and genome organization: .....	22
SARS-CoV-2 life cycle: .....	23
COVID-19 disease:.....	25
SARS-CoV-2 protease as target for the development of antivirals: ....	25
Aims.....	28
Specific aims.....	28
Methods overview.....	29
<i>In silico</i> library preparation – paper I.....	29
Molecular docking – paper I .....	29
Molecular docking – paper II .....	30
Molecular dynamics simulations – papers I and II.....	30
Q6 molecular dynamics simulations – papers I and II .....	30
Linear interaction energy calculations – paper I and II.....	31
Enzymatic assays – papers I, II .....	31
Enzymatic assays – papers III, IV .....	32
Yield reduction assays – papers III, IV .....	32
CPE-based antiviral assay – paper IV .....	33

Results and discussion .....	34
Identification of protease inhibitors against flaviviruses.....	34
Identification of active ZIKV protease inhibitor by <i>in silico</i> molecular docking and MD simulations (paper I) .....	34
Homology modeling of TBEV NS2B-NS3 protease (paper II).....	37
<i>In silico</i> modeling of TBEV protease in complex with a known pan-flavivirus protease inhibitor (paper II).....	38
Production of recombinant TBEV protease and enzyme's kinetics (paper II) .....	40
Compound <b>86</b> and similar peptidomimetics inhibits TBEV protease <i>in vitro</i> (paper II) .....	40
Identification of protease inhibitors against coronaviruses .....	43
The NO donor SNAP inhibits SARS-CoV-2 replication <i>in vitro</i> (paper III).....	43
Identification of a novel class of potent peptidomimetics inhibitors of SARS-CoV-2 main protease (paper IV) .....	44
Structure-activity relationship (SAR) study (paper IV).....	45
Antiviral activity of MP6 in Calu-3 and Caco-2 cell lines (paper IV).48	
Conclusions and future prospectives.....	49
Acknowledgments.....	51
References.....	53

# Abbreviations

CNS	central nervous system
CPE	cytopathic effect
DECL	DNA-encoded chemical libraries
DENV	dengue virus
EL	electrostatic
ER	endoplasmic reticulum
ERGIC	ER-Golgi intermediate compartment
LIE	linear interaction energy
MD	molecular dynamics
MERS-CoV	Middle east severe acute respiratory syndrome coronavirus
M <sup>pro</sup>	main protease
NO	nitric oxide
NS	non-structural
ORF	open reading frame
p-gp	p-glycoprotein
RdRp	RNA-dependent RNA polymerase
SARS-CoV	severe acute respiratory syndrome coronavirus
SARS-CoV-2	severe acute respiratory syndrome coronavirus 2
SMILES	Simplified molecular-input line-entry system
TBE	tick-borne encephalitis
TBEV	tick-borne encephalitis virus
UTR	untranslated region
vdW	Van der Waals
Vina	AutoDock Vina
WNV	West Nile virus
YFV	yellow fever virus
ZIKV	Zika virus



# Introduction

Several viruses belonging to the flavivirus genus (Flaviviridae family) and betacoronavirus genus (Coronaviridae family) are important human pathogens and represent a major current and future challenge to global public health.

Vector-borne flaviviruses cause hundreds of millions of infections worldwide. Dengue virus alone causes an estimated 96 million symptomatic infections every year<sup>1</sup>, with an associated global cost due to treatment, prevention, death and reduced productivity between \$8.9 and \$39.3 billion<sup>2</sup>. The spreading of arthropod vectors and the emergence of flaviviruses in new geographical regions with a naïve population can cause severe outbreaks, like the Zika virus outbreak in Brazil (2014-2016)<sup>3</sup>.

Likewise, zoonotic coronaviruses can emerge and spread, which has happened three times within the 21<sup>st</sup> century causing the SARS-CoV-1 outbreak of 2003, the MERS-CoV outbreak of 2012 and the SARS-CoV-2 pandemic that started in 2019<sup>4</sup> and infected and killed millions of people.

Given the potential of both flaviviruses and coronaviruses to emerge and spread causing both outbreaks and pandemic events, antiviral options are urgently needed to mitigate the current and future burden associated with these pathogens. Antivirals with broad-spectrum activity would be particularly valuable in countries with several co-circulating flaviviruses and to reduce transmission during the early stage of future outbreaks caused by novel emerging coronavirus.

Both flaviviruses and coronaviruses have structurally conserved proteases essential for the processing of viral polyproteins into mature and functional viral proteins<sup>5,6</sup>. The major aim of the research presented in this thesis was to combine several *in vitro* and *in silico* techniques to identify and validate inhibitors of Flavivirus NS2B-NS3 serine protease and Coronavirus 3CL cysteine protease (also known as the main protease or “M<sup>pro</sup>”). Particular attention was given to the identification of protease inhibitors against Zika, tick-borne encephalitis and SARS-CoV-2 viruses.

# The flavivirus genus

## Classification, structure, and genome organization:

Flaviviruses are vector-borne RNA viruses belonging to the flavivirus genus of the Flaviviridae family. Dengue (DENV), yellow fever (YFV), West Nile (WNV), Japanese encephalitis (JEV), Zika (ZIKV) and tick-borne encephalitis viruses (TBEV) are some examples of flaviviruses that can cause severe infections in humans.

Flaviviruses are characterized by having a small, enveloped virion (~50 nm in diameter) containing a single stranded positive-sense RNA genome of about 11kb composed of one open reading frame (ORF) flanked by two untranslated regions (UTR) at the 5' and 3' ends (Figure 1)<sup>7</sup>. The ORF code for three structural proteins: the capsid (C), the pre-membrane (prM) and the envelope (E) proteins, forming the virion, and seven non-structural (NS) proteins: NS1, NS2A, NS2B, NS3, NS4A/2k, NS4B, NS5 mediating viral replication, assembly, host immune response modulation and evasion<sup>7</sup>.

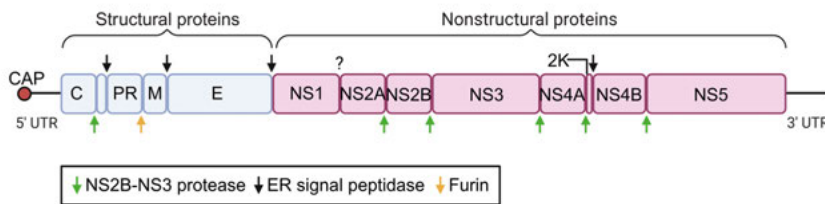


**Figure 1: Flavivirus genome organization:** The flavivirus genome is composed of one open reading frame (ORF) with a 5' cap but no 3' poly(A) tail. The ORF is translated into a single polypeptide that is cleaved at different sites into structural (blue) and non-structural proteins (red) by the viral protease (green arrow) and host proteases (black and yellow arrows). The site between NS1 and NS2A is cleaved by an unknown host protease. Figure created with biorender.com.

## Life cycle:

The viral life cycle starts with the binding of the viral E protein to its receptor on the surface of the host cell, triggering viral entry by clathrin-mediated endocytosis<sup>8,9</sup>. The acidic pH within the endosome induces conformational changes of the E protein<sup>10,11</sup> causing the fusion of the viral and endosome membrane<sup>12</sup> and the release of the nucleocapsid in the cytoplasm. The mechanism inducing the uncoating of the viral genome has not been extensively investigated, but might involve the ubiquitination of capsid proteins<sup>13</sup>, conformational changes of the capsid proteins induced by the acidic pH in endosome or interaction with ribosomes<sup>14</sup>.

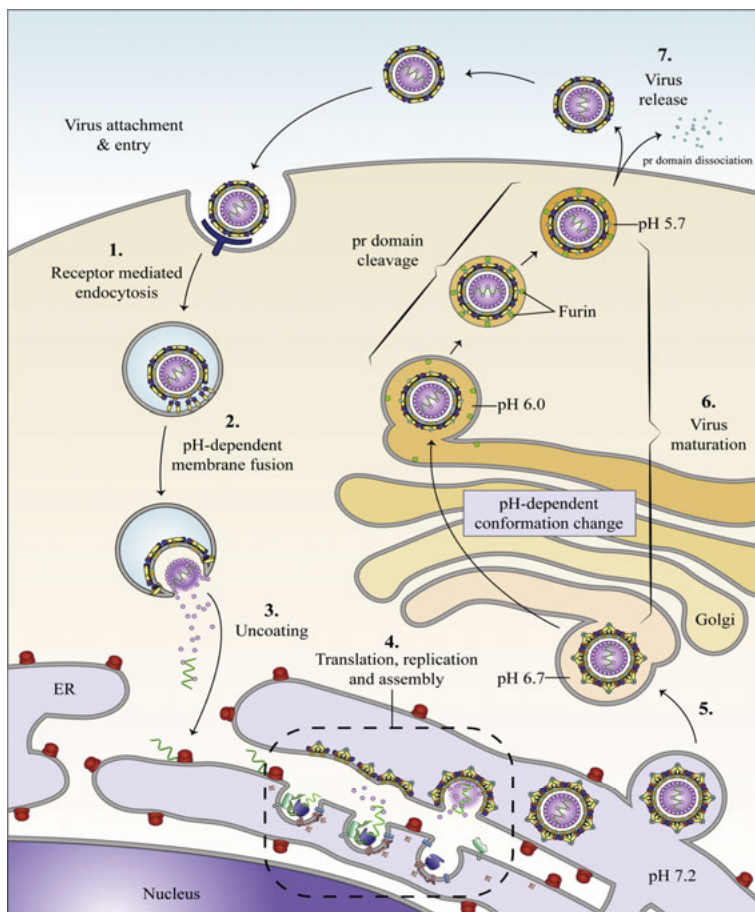


**Figure 2: Schematic representation of the life cycle of flaviviruses.** After entry and uncoating the viral genome is translated to produce structural and non-structural proteins. The non-structural proteins are responsible for reshaping the membrane of the host cell ER into replication organelles (RO). In the ROs (framed box) the viral genome is replicated and packed into assembling viral particles. Protease inhibitors prevent the maturation of viral protein, formation of ROs and replication of the viral genome stopping the virus life cycle. Figure from Nicholls et al. 2020<sup>15</sup> (used with the permission from the publisher, license number: 5601300779212).

The viral polyprotein is then processed to produce mature and functional viral proteins by host factors and by the viral NS2B-NS3 protease, consisting of the N-terminus of NS3<sup>16</sup> and the NS2B cofactor<sup>17,18</sup>. The NS proteins 1, 2, 4A and 4B induce the invagination of the rough endoplasmic reticulum (RER) to form replication organelles (RO)<sup>19</sup> where they co-localize with the viral protease helicase and RNA-dependent RNA polymerase (RdRp) promoting the replication of the viral genome<sup>20–23</sup> (Figure 2). In the ROs the viral NS5 RdRp, aided by the C-terminal NS3 helicase, first use the positive-sense RNA genome to synthesise a complementary negative-sense RNA strand that is in turn

used as template to produce several other positive-sense viral genomes<sup>24</sup>. The newly produced positive sense viral genomes are either translated to produce more viral protein or encapsidated through complementary electrostatic interactions with the positively charged capsid proteins<sup>25</sup>. New immature viral particles form when the nucleocapsid, interacting with the cytosolic portions of the prM and E proteins, buds into the endoplasmic reticulum<sup>19,26</sup>. Viral particles mature traveling along the secretory pathway to and through the Golgi where a portion of prM, masking the fusion peptide of the E protein, is cleaved and lost upon secretion from the host cell giving a mature and infectious virion<sup>27</sup>.

## Flaviviruses epidemiology and disease:

Flaviviruses are mainly transmitted through the bite of an infected arthropod vector, usually a mosquito or a tick (Figure 3). However, alternative modes of infection like sexual<sup>28</sup> and vertical<sup>29</sup> transmission have been reported for ZIKV, while consumption of contaminated unpasteurized milk<sup>30–32</sup> or cheese<sup>33</sup> is a known transmission route for TBEV and possibly also for Powassan<sup>34</sup> and Alkhurma<sup>35</sup> viruses. In the sylvatic transmission cycle non-human mammals and birds represent the reservoir for flaviviruses, while humans are dead-end hosts that can accidentally be infected through spillover events<sup>36</sup>. However, humans are the main reservoir for DENV, ZIKV<sup>37</sup> and YFV<sup>38</sup> during outbreaks in the urban environment, where the virus is transmitted from viremic infected subjects to the mosquito vector.

Early replications occur at the site of feeding in keratinocytes, fibroblasts and myeloid cells of both epidermis and dermis of the skin<sup>39–43</sup>. Infected myeloid cells like dendritic cells and Langerhans cells can migrate via the lymphatic system to a draining lymph node<sup>44–46</sup> where the virus further replicates, and enters the peripheral blood system causing viremia and dissemination to other tissues.

Infection is acute, usually asymptomatic, or self-limiting with fever, headaches, malaise/fatigue, muscle pain (myalgia) and joint pain (arthralgia). However, flaviviruses can also cause potentially fatal diseases like hemorrhagic fever, shock syndrome and encephalitis or non-lethal but long-term morbidities and fetal abnormalities.

Flaviviruses are found on all continents (except for Antarctica) where they are mainly spread by mosquitoes of the *Aedes* and *Culex* genera<sup>47</sup> and ticks of the *Ixodes*, *Dermacentor* and *Haemaphysalis* genera<sup>48–52</sup>. Given their wide distribution, especially around the equator in highly populated developing countries, flaviviruses represent a major public health threat. The highest disease burden in terms of yearly symptomatic infections and deaths is caused by DENV with ~96 million cases and ~40,000 deaths<sup>1,53</sup>, followed by YFV that causes 109,000 cases of which 51,000 are fatal<sup>54</sup>.



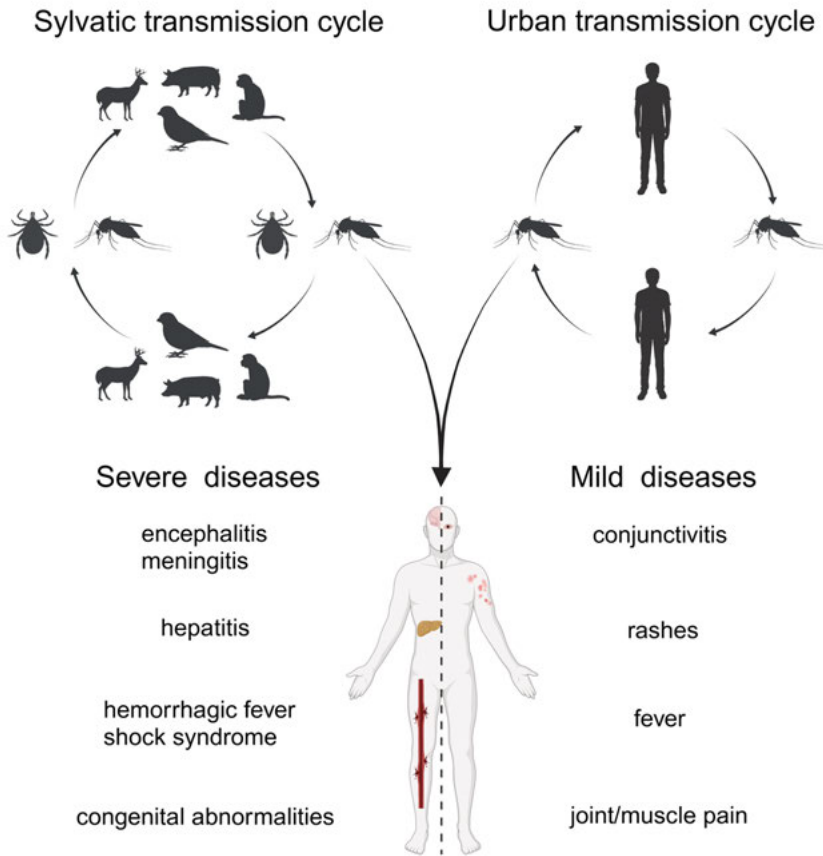


**Figure 3: Flaviviruses transmission cycle and examples of disease manifestation in humans:** Flaviviruses are transmitted in the wild between feeding vectors, usually a tick or a mosquito and amplifying reservoirs, usually a non-human mammal or bird. The transmission cycle of ticks involves different development stages (larva, nymph, and adult) and one or more hosts of different size<sup>55</sup>. For the sake of simplicity, only the adult form is shown in this diagram. Flaviviruses can spill over from the sylvatic cycle and infect humans that are usually dead-end host due to low viremia. However, urban transmission of flaviviruses from viremic humans to mosquitoes have been reported for DENV, YFV and ZIKV. When symptomatic, flavivirus infection can cause mild flu-like symptoms or potentially fatal hemorrhagic and neurotropic diseases. Figure created with Biorender.com.

In Europe, the majority of flavivirus infections in humans are caused by TBEV<sup>56</sup> and WNV<sup>57</sup>, responsible for 2559 and 358 cases per year, respectively (average number of yearly confirmed cases over the period 2012-2021, data from ECDC<sup>58</sup>). Usutu virus, that emerged in Europe no later than 1996<sup>59</sup>, is now also endemic in several European countries where it causes sporadic infections in humans<sup>60</sup>. Other important human pathogens like DENV and ZIKV have the potential to cause outbreaks in south/central Europe where *Aedes*

*albopictus*, a permissive mosquito vector for both viruses, is already established<sup>61,62</sup>. Outbreaks of DENV with autochthonous transmission have been reported in Croatia (2010)<sup>63</sup>, France (2010 and 2013)<sup>64,65</sup>, Portugal (2012-2013)<sup>66</sup> and Italy (2020)<sup>67</sup>. In the future, the scale and frequency of DENV outbreaks may increase due to more favorable climatic conditions supporting higher levels of viral replication within the vector and more efficient transmission. However, the lack of a suitable non-human primate reservoir could prevent DENV or ZIKV from becoming endemic within the European territory. Unfavorable ecological dynamics have been described for JEV that, despite being detected in *Culex pipiens* mosquitoes<sup>68,69</sup> and birds in Italy<sup>70</sup>, have not yet caused any case of human infection. Low vector or bird host competence or lack/low availability of other amplifying hosts have been proposed as causes currently preventing JEV emergence<sup>70</sup>.

## Zika virus

ZIKV was first isolated in Africa in 1947 from Rhesus monkeys located in the forest of Zika (Uganda)<sup>71</sup>, and was isolated in humans in 1954 during a suspected yellow fever outbreak in Nigeria<sup>72</sup>. ZIKV was later (1969) isolated also in Asia from *Aedes aegypti* mosquitoes collected in Malaysia<sup>73</sup>, but serological studies proved that ZIKV has been circulating in India, Malaysia and Borneo since at least the early 1950s<sup>74,75</sup>. Phylogenetic analyses of ZIKV full genomic nucleotide sequences showed that African and Asian isolates clustered separately, leading to the broad classification of ZIKV into the African and Asian genotypes<sup>76,77</sup>.

Although ZIKV was circulating in Africa and Asia, only 15 cases of human ZIKV infection were reported in the literature<sup>72,76–79</sup> during the fifty-two years that followed the first reported cases in 1954. Fever, joint pain, pain behind the eyes and malaise were the common symptoms reported in these 15 cases, which are consistent with general symptoms associated with flavivirus acute infections<sup>72,78–80</sup>. The likely underreporting of ZIKV cases could be explained by the high rate (~ 80%) of asymptomatic cases<sup>81,82</sup> and the mildness of the disease that could be easily misdiagnosed for another infection caused by a mosquito-borne virus co-circulating in the area of interest.

In 2007, the Asian strain of ZIKV<sup>77,82,83</sup> emerged in the Yap state of the Federated States of Micronesia causing the first major ZIKV outbreak that resulted in 45 confirmed cases out of 5005 estimated total infections<sup>82</sup>. During 2013 and 2014, ZIKV kept spreading in the Pacific causing outbreaks in French Polynesia (19.000 suspected cases, 2013)<sup>83</sup>, Cook island (>900 suspected cases, 2014)<sup>84</sup>, New Caledonia (1385 confirmed cases, 2014)<sup>85</sup>, Easter Island (89 suspected, 51 confirmed cases, 2014)<sup>86</sup>. The chain of outbreaks in the Pacific was followed by the spreading of ZIKV in Brazil where the first cases were reported in early 2015<sup>87</sup>. The Brazilian outbreak (2015-2016) is the

most severe recorded to date with between 440,000 and 1,300,000 potential ZIKV cases as predicted by the Brazilian ministry of health by the end of 2015<sup>88</sup>. By February 2016 ZIKV swept through south and central Americas prompting the World Health Organization (WHO) to declare ZIKV a public health emergency of international concern<sup>89</sup>. By the summer of 2016 ZIKV reached north America where four cases of suspected autochthonous transmission of ZIKV were reported in Florida, USA<sup>90</sup>. As of February 2022, the WHO reported 89 countries and territories where autochthonous transmission of ZIKV had been documented<sup>91</sup>.

During the outbreaks caused by the Asian strain of ZIKV from 2007 onward, symptoms not observed before such as rashes and conjunctivitis were commonly reported<sup>82,83,87</sup>. More importantly, reports of severe neurological manifestations like Guillain-Barré syndrome<sup>92-94</sup>, microcephaly and other congenital cerebral malformations were reported in areas with ongoing or previous ZIKV outbreaks<sup>3,95,96</sup>. The association between ZIKV infection and vertical transmission resulting in fetal brain abnormalities was proven with the detection of ZIKV genome and protein in placenta, amniotic fluid, and fetus brains tissue<sup>97,98</sup>. Isolation of ZIKV viral particles from fetal brain samples has also been reported<sup>29</sup>. The long-term costs of the ZIKV pandemic in Latin America and Caribbean due to microcephaly, other ZIKV associated congenital abnormalities and Guillen-Barré syndrome have been estimated between \$3.2-39 billions<sup>99</sup>. This includes lifelong support to children with microcephaly, that will never join the labor force, as well as well parents (often the mother) not joining or withdrawing from the labor force<sup>99</sup>.

## Tick-borne encephalitis virus

TBEV is the causative agent of Tick-borne encephalitis (TBE), a potentially lethal disease that affect the central nervous system (CNS)<sup>100</sup>. TBEV spreads mainly through the bite of infected ticks of the *Ixodes* genus<sup>52</sup>, but consumption of unpasteurized milk from infected animals also represent a route of transmission<sup>101</sup>. There are three TBEV subtypes based on genomic variations<sup>102</sup>, with different geographical distribution in the Eurasian continent. The European subtype is mainly located in central-east and northern Europe and is transmitted mainly by ticks of the *Ixodes ricinus* species<sup>52</sup>. The Siberian subtype can be found in Siberia, Baltics and Finland where it is mainly transmitted by ticks of the *I. persulcatus* species<sup>52</sup>. The Far-Eastern subtype is found in Far-East Russia and East Asia and is transmitted by ticks of the *I. persulcatus* and *I. ovatus* species<sup>52,103</sup>.

TBEV incubation time is usually between 7-14 days and infections are usually asymptomatic with one out of four cases presenting flu-like symptoms like fever, headache, nausea, joint pain (arthralgia)<sup>100</sup>. Symptomatic cases can progress to involve the CNS causing meningitis, encephalitis, and myelitis.

Infections with the TBEV European subtype are biphasic and severe neurological symptoms develop after a brief asymptomatic period that follows the initial flu-like form of the disease<sup>104</sup>. The Siberian and Far-Eastern subtypes present a monophasic course with direct progression of the disease and development of neurological symptoms<sup>100</sup>. Severe meningoencephalitis can lead to death and long-term sequelae. The fatality rate associated with TBEV infection is highest for the Far-eastern subtype (up to 20%)<sup>100</sup> compared to the European (<1%)<sup>104</sup> and Siberian (2-3%)<sup>105</sup> subtypes. Severe long-term morbidities like fatigue, ataxia, hearing loss, decreased memory, difficulties concentrating and mental illnesses are often observed after severe TBE cases<sup>104</sup>. In follow up studies from Sweden<sup>106</sup> and Lithuania<sup>107</sup>, symptoms were still present one year post infection in 40% and 46% of the TBE patients, respectively. Although two vaccines are available, TBEV is the most important flavivirus infection in Europe. The latest data available from the ECDC show that on average over seven times more confirmed cases of TBE (2559 cases) are reported every year, as compared to WNV (358 cases)<sup>58</sup>. In 2021, most cases of TBE outside Sweden were reported in Czechia (589), Germany (417) and Lithuania (365)<sup>58</sup>. In Sweden, TBEV cases has been increasing for the past twenty years and the highest number of locally acquired cases ever recorded was 514 during 2021<sup>108</sup>.

## Flavivirus protease as target for the development of antivirals

Flaviviruses have a positive-sense RNA genome that functions as mRNA and is directly translated into a singular polyprotein that is cleaved into mature and functioning structural and non-structural proteins by the viral NS2B-NS3 protease and host factors. The flavivirus protease is a heterodimeric chymotrypsin-like serine protease composed of the NS3 N-terminal protease and the NS2B cofactor<sup>109</sup> (Figure 4A). The NS3 protease contains a His51-Asp75-Ser135 catalytic triad and is formed by two  $\beta$ -barrel domains, each containing six  $\beta$ -strands. The NS2B cofactor, and in particular approximately 40 amino acids in the central region of NS2B, are essential for the protease activity<sup>110</sup>. This NS2B core region wraps around NS3 with its C-terminus  $\beta$ -hairpin forming part of the protease active site in what is called the protease close conformation<sup>109,111</sup>. Flavivirus proteases are conserved at sequence and structural levels within the flavivirus genus<sup>112,113</sup> and recognize similar substrates characterized by a positively charged amino acid, like arginine or lysine, in the P1 and P2 positions (two residues positioned before the cleavage site) and a small amino acid, like glycine or serine, in the P1' (amino acid positioned after the cleavage site) position<sup>114</sup> (Figure 4C).

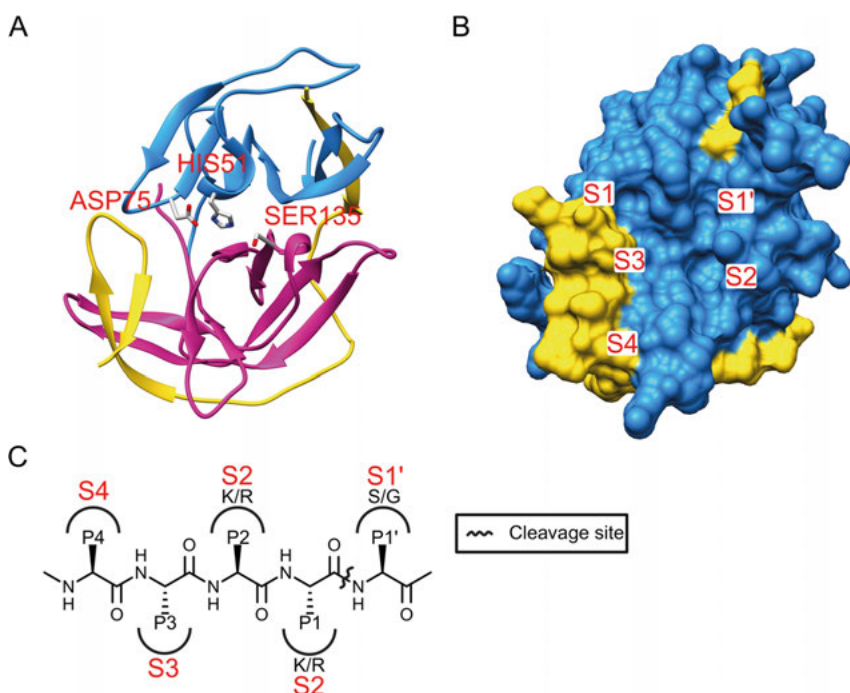


**Figure 4: Structure and substrate specificity of the flavivirus protease.** (A) The enzyme catalytic triad formed by residues ASP75, HIS51 and SER135 is placed at the interface of two  $\beta$ -barrel domains (shown in blue and magenta) forming NS3. In the active form of the protease, the NS2B cofactor (shown in yellow) wraps around NS3. (B) The surface of the NS2B-NS3 protease showing the five subsites (S4, S3, S2, S1 and S1') that form the binding pocket of the enzyme. The NS3's surface is shown in blue and the NS2B's surface is shown in yellow. (C) Schematic representation of the flavivirus protease substrate showing residues positioned before (P4-P1) and after the cleavage site (P1'). The subpacket of the binding site occupied by each residue is also shown in red. All flavivirus proteases recognize substrates having a positively charged residue (lysine or arginine) in P1 and P2 before the cleavage site, and a small residue (serine or glycine) in P1'. Figures A and B were made with Chimera<sup>115</sup> using ZIKV protease crystal structure with Protein Data Bank ID (PDBID) 5GPI<sup>116</sup>. Figure C was created with Biorender.com.

The NS2B-NS3 protease is indispensable for the virus replication, and it has been extensively studied as a suitable target for the development of antiviral prophylaxis/treatment<sup>117–123</sup>. Moreover, the flavivirus NS2B-NS3 protease becomes an even more attractive target when considering that it is structurally conserved within the genus flavivirus, theoretically allowing the design of pan-flavivirus protease inhibitors. However, efforts in identifying inhibitors of NS2B-NS3 protease has been hampered by the shallow and solvent exposed active site<sup>111</sup> (Figure 4B). The presence of aspartate residues close to the S1 and S2 pocket also limited for a long time the design of potent pan-flavivirus inhibitors to basic peptide-hybrid compounds with low cell membrane

permeability and metabolic stability<sup>124–126</sup>. Macrocyclization of peptides can help targeting shallow surfaces and can improve both metabolic stability and cell permeability<sup>127</sup>. However, reported macrocycles based on basic peptides with potent *in vitro* inhibitory activity of ZIKV, WNV and DENV recombinant proteases<sup>128,129</sup> had low antiviral effect in cell-based assays so far<sup>129</sup>. Sub-micromolar antiviral activity in cell-based assay was finally achieved against DENV by a new class of non-charged small molecules with promising drug-like properties<sup>130,131</sup>.

## SARS-CoV-2

### Classification, structure, and genome organization:

SARS-CoV-2 is a positive-sense RNA virus belonging to the orthocoronavirinae subfamily of the Coronaviridae family<sup>132</sup>. The orthocoronavirinae subfamily is divided into four genera: alfa, beta, gamma, and delta coronaviruses. Human pathogens are found in the alfa and beta coronaviruses genera, while the gamma and delta genera cause infection in non-human mammalian and avian species<sup>133</sup>. SARS-CoV-2 and the other highly pathogenic severe acute respiratory syndrome coronavirus (SARS-CoV) and the Middle East respiratory syndrome coronavirus (MERS-CoV) group together in the betacoronaviruses genus. Human coronaviruses (HCoV) responsible for seasonal mild respiratory tract infections are found in both the alfa (HCoV 229E and NL63) and the beta (HCoV OC43 and HKU1) coronavirus genera.

The SARS-CoV-2 virion is spherical and enveloped with an average diameter of  $\sim 90$  nm<sup>134</sup>. The viral genome is composed of a single stranded positive-sense RNA of  $\sim 30$ kb containing 14 ORF with two UTR at both ends comprising a 5' cap and a 3' poly(A) tail<sup>135</sup>. Two main ORF “1a” and “1b” codes for 15 NS proteins, ten coded in ORF1a (NS1-10) and five coded in ORF1b (NS12-16)<sup>135</sup>. The remaining 12 ORF code for the four structural proteins: spike (S), envelope (E), membrane and nucleocapsid, plus eight accessory proteins<sup>135</sup>.

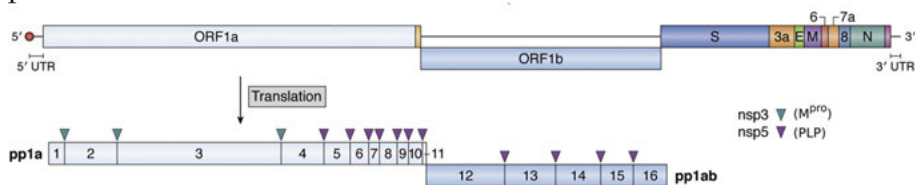


**Figure 5: SARS-CoV-2 genome organization.** The genome of SARS-CoV-2 is composed of six main ORFs coding for the structural and non-structural proteins. The ORF 1a and 1b are translated into two polyproteins that are processed by the viral main (M<sup>pro</sup>) and the papain-like (PLP) proteases. Figure adapted from Grellet et al. 2022<sup>136</sup>, under creative commons attribution CC BY 4.0.

## SARS-CoV-2 life cycle:

SARS-CoV-2 entry is initiated by the interaction between the receptor binding domain in the S1 subunit of the S protein and the angiotensin converting enzyme 2 (ACE2) on the host cell surface<sup>137</sup>. Following the interaction between S1 and ACE2, cell entry can occur via the direct fusion of the viral and cell membranes (cell surface entry pathway) or via endocytosis with subsequent fusion of the viral and endosome membranes (endosomal entry pathway). In both pathways, the proteolytic processing of the S protein is required to expose the S2 fusion peptide and sets in motion conformational changes that lead to membrane fusion<sup>138,139</sup>. In lung and gastrointestinal cells, the transmembrane serine protease 2 (TMPRSS2) cleaves the S protein at the S2' site causing the viral and cell membrane to fuse<sup>137,140</sup>. The processing of the S protein by furin or other protein convertases at a second site referred to as S1/S2 is a prerequisite for the efficient processing of S2' by TMPRSS2<sup>137,140</sup>. It is important to note that the furin cleavage of the S1/S2 site seems to occur before the newly produced viral particles exit the infected cells<sup>141,142</sup> and that these newly produced particles are already primed at the S1/S2 site when they bind to ACE2. In cells not expressing TMPRSS2, viral entry occurs through endocytosis and the S protein is processed by endosomal cathepsin L protease at, or near, the S2' site<sup>143–145</sup>. After the nucleocapsid is released, the viral genome is uncoated and directly translated by cytoplasmic ribosomes. At this stage only the ORF 1a and 1b are translated, giving two polyproteins (pp1a and pp1ab) containing all non-structural proteins necessary for the replication of the viral genome. The two viral polyproteins are proteolytically processed into fifteen mature and functional proteins by the viral papain-like protease (NS3) and the main protease (NS5)<sup>146</sup>. The non-structural (NS) protein NS1 shuts down the host translation, while NS3, NS4 and NS6 induce the formation of replication organelles (ROs) by remodeling the ER into convoluted membranes and double-membrane vesicles (DMVs)<sup>147,148</sup>. In the DMVs the viral genome is replicated<sup>149,150</sup> by the NS12 RdRp together with the NS13 helicase, the NS14 proofreading 3'-5' exonuclease and other NS proteins with enzymatic or supportive roles<sup>151</sup>. The viral replication starts with the synthesis of a full-length negative-sense genomic RNA that is later used as template to produce more positive-sense viral genomes for encapsidation or translation of more NS proteins.

During the synthesis of full-length negative-sense genomic RNAs, eight different negative-sense sub-genomic RNAs coding for structural and accessory proteins are also synthesized. In order to be translated, these sub-genomic RNAs are first used to produce complementary positive-sense sub-genomic "mRNAs" that leave the DMVs through pores<sup>152</sup>. The E, M and S structural proteins are translated by ribosomes located on the surface of the ER, inserted in the ER membrane, and accumulate at the ER-Golgi intermediate compartment (ERGIC)<sup>153</sup>. The N structural protein is translated by free

ribosomes in the cytoplasm where it binds with viral genomic RNA exiting from the DMVs' pore to form the nucleocapsid<sup>154</sup>. Virions assembly is completed when the nucleocapsid interact with the M protein and buds into the lumen of the ERGIC acquiring a membrane with the remaining viral structural proteins<sup>149,154</sup>. The newly produced viral particles exit the cells through exocytosis of deacidified lysosomes rather than the constitutive secretory pathway<sup>155,156</sup>.

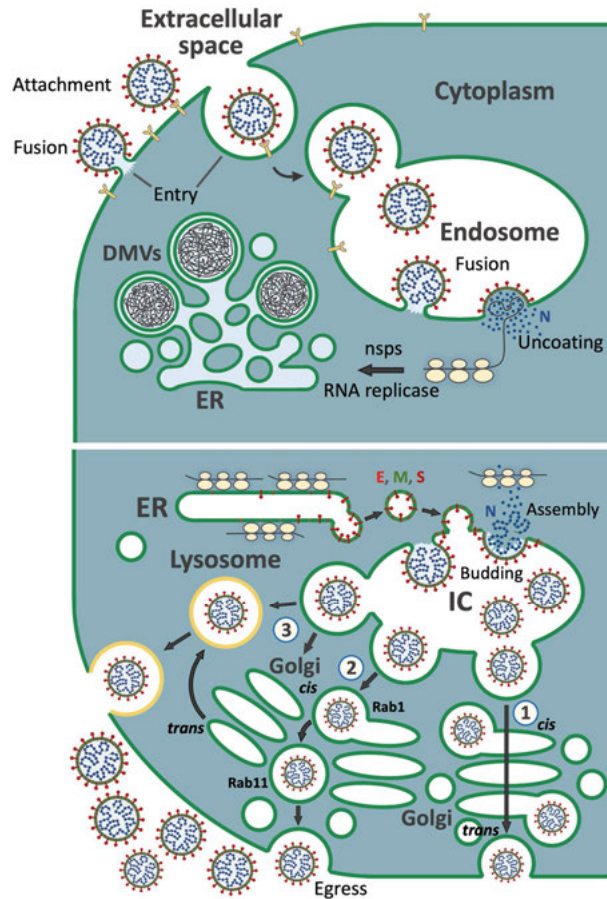


**Figure 6: Schematic representation of SARS-CoV-2 life cycle.** After entry and uncoating the viral genome is translated into the viral polyproteins 1a and 1ab containing all non-structural proteins. The two polyproteins are cleaved by the viral main and papain-like proteases into mature non-structural proteins responsible for reshaping the membrane of the host cell ER into double membrane vesicles (DMVs). In DMVs viral genome is replicated, protease inhibitors prevent the maturation of viral non-structural protein, formation of DMVs and replication of the viral genome stopping the virus life cycle. Figure from Prydz et al. 2022<sup>153</sup>, used under creative commons attribution CC BY NC ND 4.0.



## COVID-19 disease:

SARS-CoV-2 emerged in China at the end of December 2019 where it caused a cluster of severe pneumonia cases linked to a wet market in the city of Wuhan<sup>157,158</sup>. The virus quickly spread around the world overwhelming hospitals and prompting the introductions of lockdowns and travel restrictions to reduce the transmission of the virus. Human SARS-CoV-2 infection, referred to as COVID-19, can be asymptomatic or manifest with both mild and severe disease after an incubation period of 4 to 7 days<sup>159</sup>. Initial symptoms are typical of an acute respiratory infection and include fever, sore throat, cough, fatigue, and joints/muscles pain (arthralgia/myalgia)<sup>159</sup>. COVID-19 severe manifestations are caused by the spreading of the infection into the lower respiratory tract causing shortness of breath and hypoxemia<sup>160</sup>. The resulting pneumonia, combined with a strong immune response can lead to the development of acute respiratory distress syndrome (ARDS). ARDS is a life-threatening condition characterized by extensive tissue damage reducing the lungs gas exchange capacity causing severe systemic hypoxemia<sup>161,162</sup>. The omicron variants<sup>163</sup> and related subvariants of concern have shorter incubation time (3 to 4 days)<sup>164</sup> and cause less severe infections<sup>165–167</sup> mostly limited to the upper respiratory airways. This change in tropism have been connected to a less efficient use of the “cell surface entry” pathway, that relies on TMPRSS2 for the priming of the virus spike protein<sup>168–171</sup>.

## SARS-CoV-2 protease as target for the development of antivirals:

SARS-CoV-2 codes for a viral 3-chymotrypsin-like cysteine protease (3CLpro) also known as main protease (M<sup>pro</sup>)<sup>172</sup> that cleaves the two viral polypeptides pp1a and pp1ab at 11 sites<sup>146</sup> and is therefore essential for the viral replication. SARS-CoV-2 codes also for a papain-like protease (PL protease) that also process the viral polypeptides at three sites and can be used as target for the development of inhibitors<sup>173</sup>. Active M<sup>pro</sup> assembles into a homodimer with each subunit containing three domains (Figure 2). Domains I and II fold into two  $\beta$ -barrels formed by six  $\beta$ -strands while domain III regulates dimerization (Figure 7). The enzymes catalytic dyad (His41 and Cys145) is placed in a grove at the interface of domains I and II where it catalyzes the cleavage of its substrate at sites with sequence LQ↓S/A<sup>174</sup>. M<sup>pro</sup> is structurally conserved within the coronavirus family (Figure 7). This allowed for the design of pan-coronavirus protease inhibitors<sup>175</sup> and provided starting points to jumpstart the effort for the design of inhibitors against SARS-CoV-2 protease<sup>172</sup>. As a result, several protease inhibitors designed against SARS-CoV-2 were also found to be active against SARS-CoV, MERS-CoV and other human coronaviruses like 229E<sup>176–178</sup>.

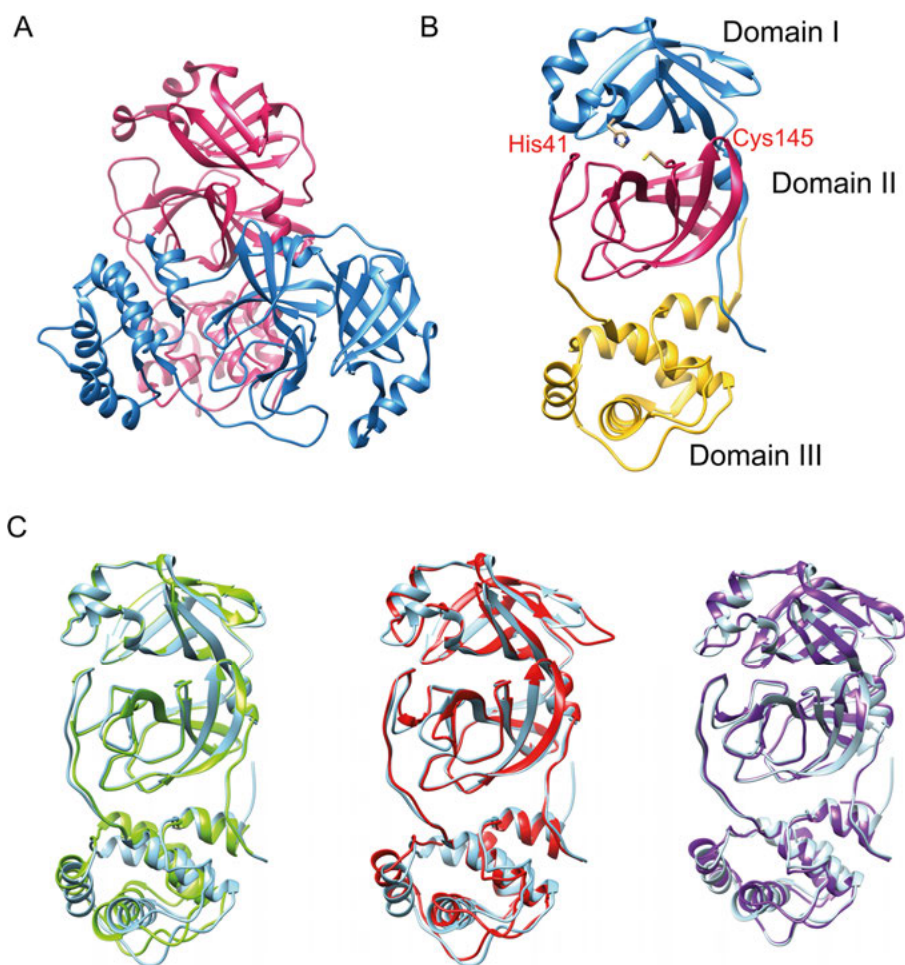


**Figure 7: Structure of coronavirus proteases.** (A) Homodimer of SARS-CoV-2 protease formed by identical subunits (shown in blue and magenta). (B) A single SARS-CoV-2 M<sup>pro</sup>. The active site of the protease, where the catalytic dyad (His41 and Cys145) is located, is position between the first two domains (shown in blue and magenta). (C) Structural comparison of SARS-CoV-2 M<sup>pro</sup> (light blue, PDBID 7PFM) aligned with SARS-CoV (green, PDBID 7K0H), MERS-CoV (red, PDBID 4RSP) and HCoV-229E (purple, PDBID 2ZU2). Figure made with Chimera<sup>115</sup>.

Since late 2021, infections have been driven by several waves of new SARS-CoV-2 Omicron variants of concern. Although the risk of death from Omicron infection is lower as compared to the previous delta variant, complication leading to hospitalization and death still occur<sup>179,180</sup>. Although mRNA vaccines have been instrumental in reducing severe disease and hospitalization, achieving long term immunity seems to be challenging due to immune escape<sup>181–183</sup> and rapid decline of antibody titer over time<sup>182,184</sup>. Therefore,

antiviral options for the prevention and treatment of SARS-CoV-2 infection in immunosuppressed and high-risk subjects are necessary to reduce COVID-19 health burden. Moreover, broad-spectrum antivirals active against several coronavirus will be instrumental for preventing or mitigating the next pandemic by reducing early transmission and providing a starting point for the development of more potent compounds if necessary. The feasibility of Mpro inhibitors as prophylaxis or treatment for SARS-CoV-2 infections has already been proven. Currently there are two protease inhibitors approved for the treatment of mild to moderate infection in subjects at risk of progression to severe COVID-19 disease: Paxlovid and Xocova. Both the EMA (European Medicine Agency) and FDA (Food and Drug Administration) have approved or provided emergency use authorization to Paxlovid<sup>185</sup>, a combination of nirmatrelvir<sup>177</sup> (the active SARS-CoV-2 protease inhibitor) and ritonavir (a HIV-1 protease inhibitor used as booster). Ensitralvir<sup>178</sup>, also administered orally, have so far only been approved in Japan by the Japanese Ministry of Health Labour and Welfare (MHLW) under the name Xocova<sup>186</sup>

# Aims

The general aim of this thesis was to identify novel inhibitors of flavivirus and coronavirus proteases with a focus on Zika, tick-borne encephalitis and SARS-CoV-2 viruses.

## Specific aims

- Paper I: Identify and test protease inhibitors against ZIKV protease using a combination of *in silico* and *in vitro* methods. The establishment of relevant *in silico* and *in vitro* methods to identify and confirm the activity of protease inhibitors was also part of the aim of this sub-project.
- Paper II: Model the NS2B-NS3 protease of TBEV for which a crystal structure is not currently available. Use of the modeled structure in combination with the *in silico* and *in vitro* methods established in paper I to identify and test protease inhibitors of the TBEV protease.
- Paper III: Study the antiviral activity of the nitric oxide donor SNAP against SARS-CoV-2 replication. The main protease of SARS-CoV-2 was evaluated as the potential target of SNAP inhibition.
- Paper IV: Identify novel and potent inhibitors of SARS-CoV-2 main protease using state of the art DNA-encoded chemical library technology.

## Methods overview

This section contains a brief description of the main methods used to facilitate the reading of the next section where the main results from the four studies comprised in this thesis are summarized. Detailed information can be found in the original papers.

### *In silico* library preparation – paper I

SMILES (simplified molecular-input line-entry system) of 8222 protease inhibitors were collected from the MEROPS small-molecule inhibitor database<sup>187</sup> and the PubChem database<sup>188</sup>. The library was filtered using OpenBabel v2.3.2 to remove small fragments with molecular weight lower than 180 Da. The 3D structures of the remaining 6225 compounds were generated, and used for *in silico* screening.

### Molecular docking – paper I

The library composed of the 3D structures of 6265 compounds was screened in parallel by molecular docking using iGEMDOCK v2.1<sup>189</sup> and AutoDock Vina v1.1.2<sup>190</sup> (Vina). While iGEMDOCK can sequentially dock all compounds in a library, Vina docks one compounds at the time. AUDocker v1.1.2<sup>191</sup> was used to automate the docking of all compounds in the library when using Vina. The library screening was performed using ZIKV crystal structure with PDBID 5LC0<sup>192</sup>. The searching space (i.e. the area where the programs try to fit the compounds) was automatically centred on ZIKV protease binding site by iGEMDOCK, while for Vina the searching space was manually defined using AutoDockTools (v1.5.6) to a box (30x30x30 Å) encompassing the ZIKV protease binding site. Vina was also used to dock compound **9b** against ZIKV 5GPI<sup>116</sup> and 5GJ4<sup>122</sup> crystal structures and compound **86** against ZIKV 5GPI crystal structure.

## Molecular docking – paper II

Vina was used to dock compound **86** with DENV (PDBID 3U1I)<sup>111</sup>, WNV (PDBID 5IDK)<sup>126</sup> and ZIKV (PDBID 5GPI)<sup>116</sup> and TBEV (our own model) proteases. The searching space was again defined by a virtual box (30x30x30 Å) encompassing the binding site of the proteases as described above.

## Molecular dynamics simulations – papers I and II

Molecular dynamics (MD) simulations were performed as previously described (Akaberi et al. 2018)<sup>193</sup> using GROMACS v5.1.1<sup>194</sup>. All systems composed of a flavivirus protease in complex with a compound were set up following the same steps. First, topologies for proteases and compounds were generated using the AMBER99SB-ILDN<sup>195</sup> and general AMBER<sup>196</sup> force fields, respectively. The force fields contain all information necessary to describe how atoms interact within and between molecules and therefore how the system evolves over time. The system was then placed in the middle of a virtual dodecahedron box, solvated using the TIP3P water model, and charges were equilibrated adding sufficient  $\text{Na}^+$  and  $\text{Cl}^-$  ions. Before starting the simulations, the system was energy minimized, assigned random starting velocities, and equilibrated to an average temperature of 300K (27°C) and pressure of 1bar. Four simulations of 40ns were run for each protease-compound complex as well as for the proteases alone. A “snapshot” of the system was saved every 10ps. The resulting trajectories were analyzed using GROMACS built-in tools.

## Q6 molecular dynamics simulations – papers I and II

Q6<sup>197</sup> was used to run molecular dynamics simulations of flavivirus protease-compound complexes and free (unbound) compounds in solution (water). The topologies for complexed protease-compounds and compounds free forms were generated using the OPLS-AA force field<sup>198</sup>. The systems were placed in a simulation sphere, solvated by adding the TIP3P water model, and slowly equilibrated at a temperature of 310K (37 °C). The net-charge of the proteases was made neutral by changing selected charged residues to their neutral form. Five simulations of 5ns with different starting velocities were performed for each system and the ligands surrounding energies were saved every 25fs.

## Linear interaction energy calculations – paper I and II

The linear interaction energy method (LIE) was used to calculate the free binding energy of compounds using the equation (1)<sup>199</sup>.

$$\Delta G_{\text{bind}}^{\text{calc}} = \alpha \Delta \langle U_{\text{l-s}}^{\text{vdW}} \rangle + \beta \Delta \langle U_{\text{l-s}}^{\text{el}} \rangle + \gamma \quad (1)$$

In (1) ( $\Delta G_{\text{bind}}^{\text{calc}}$ ) is equal to the sum of the average ligand surrounding (l-s) Van der Waals ( $\langle U_{\text{l-s}}^{\text{vdW}} \rangle$ ) and electrostatic ( $\langle U_{\text{l-s}}^{\text{el}} \rangle$ ) interactions. These two terms were calculated as shown in (2) and (3) from the difference of average Van der Waals (vdW) and electrostatic (el) ligand surrounding interactions energies extracted from MD simulation performed with ligands bound to a protease (p) or free in water (w).

$$\Delta \langle U_{\text{l-s}}^{\text{vdW}} \rangle = \langle U_{\text{l-s}}^{\text{vdW}} \rangle_p - \langle U_{\text{l-s}}^{\text{vdW}} \rangle_w \quad (2)$$

$$\Delta \langle U_{\text{l-s}}^{\text{el}} \rangle = \langle U_{\text{l-s}}^{\text{el}} \rangle_p - \langle U_{\text{l-s}}^{\text{el}} \rangle_w \quad (3)$$

The scaling factor “ $\alpha$ ” was set to 0.18 and “ $\beta$ ” was set to 0.33 for the compound 9b ( $\geq 2$  OH groups) and 0.5 for the charged compound **86**<sup>200, 201</sup>. The constant term  $\gamma$  was set to 0.

## Enzymatic assays – papers I, II

The inhibitory activities of compounds against recombinant ZIKV and TBEV proteases were tested using a FRET-based enzymatic assay. Different concentrations of compounds were incubated with ZIKV (final concentration 3 nM) or TBEV (final concentration 100 nM) proteases for 10 minutes at room temperature in assay buffer (20 mM Tris-HCl pH 8.5, 10% glycerol and 0.01% Triton X-100). The reaction was started by adding the FRET substrate Bz-Nle-Lys-Arg-Arg-AMC (Bachem Holding AG, Switzerland) at a final concentration of 20  $\mu\text{M}$  (ZIKV assays in paper I), 15  $\mu\text{M}$  (ZIKV assays in paper II) or 40  $\mu\text{M}$  (TBEV assays in paper II). The cleavage of the substrate and resulting increase in relative fluorescence units (RFU) was measured every 60 seconds for 30 minutes (paper I) or 40 minutes (paper II) using a Tecan Infinite M200 PRO plate reader (Tecan Trading AG, Switzerland). Excitation and emission wave lengths were set to 380nm and 460nm, respectively. The emitted RFU per second were plotted and used to calculate the initial velocities that were normalized to the controls (control wells with no substrate = 100% inhibition and control wells with no inhibitor = 0% inhibition). Normalized values expressed as % of protease activity inhibition were used to determine

the compounds  $IC_{50}$  by non-linear regression using the model “log(inhibitor) vs. normalized response – Variable slope” with equation:  $Y=100/(1+10^{((\text{Log}IC_{50}-X)*\text{HillSlope}))}$ .

In paper II,  $K_m$  and  $K_{cat}$  were determined by incubating recombinant ZIKV (3nM) and TBEV (100nM) proteases with the FRET substrate at concentration ranging from 4.69 to 150  $\mu\text{M}$ . The measured RFU values were converted to product concentration using a standard curve of free unquenched fluorophore of the substrate (AMC). Initial velocities were calculated and used to calculate  $K_m$  and  $K_{cat}$ .

All analysis were performed using GraphPad Prism v.6 (GraphPad Software, La Jolla California, USA).

## Enzymatic assays – papers III, IV

The inhibitory activity of compounds against recombinant SARS-CoV-2  $M^{pro}$  was tested using a FRET-based enzymatic assay. Different concentrations of compounds were incubated with SARS-CoV-2  $M^{pro}$  (final concentration  $WT_{M^{pro}}$  100nM,  $E116V_{M^{pro}}$  500nM) and incubated for 10 minutes at room temperature in assay buffer. The assay buffer used in paper III was: 20 mM Tris-HCl pH 7.5, 0.01% Triton X-100. The assay buffer used in paper IV was: 20 mM HEPES pH 7.5, 0.01% Triton X-100. The reaction was started by adding the FRET substrate DABCYL-Lys-Thr-Ser-Ala-Val-Leu-Gln-Ser-Gly-Phe-Arg-Lys-Met-Glu-EDANS (Bachem Holding AG, Switzerland) at a final concentration of 20  $\mu\text{M}$ . The cleavage of the substrate and resulting increase in relative fluorescence units (RFU) was measured every 60 seconds for 35 minutes (paper III) or 40 minutes (paper IV) using a Tecan Infinite M200 PRO plate reader (Tecan Trading AG, Switzerland). Excitation and emission wavelength were set to 355 nm and 538 nm. Data were normalized as % of protease activity inhibition and  $IC_{50}$ s calculated as describe in the previous paragraph using GraphPad Prism v.9.5.1 (GraphPad Software, La Jolla California, USA).

## Yield reduction assays – papers III, IV

In paper III, confluent Vero E6 cells seeded in 12-well plates were infected with SARS-CoV-2 (Swedish isolate from Nissen et al. 2020)<sup>202</sup> at a final MOI of 0.005, and treated with different concentrations of NAP or SNAP. Every 4 hours (h) up to 36 hours post infection (hpi) the cell media was collected, and cells re-treated. After the last re-treatment cell media was collected further collected at 48 and 72hpi and replaced with cell media with no added NAP or SNAP. Cell media was also collected from treated but not infected controls and untreated but infected controls.



In paper IV, Caco-2 cells were seeded one day prior to the assay at a density of 20.000 cells/well in 96-well plates. After overnight incubations cells were infected for 1h with 200 plaque forming units (~ MOI 0.01) of SARS-CoV-2 (Swedish isolate from Ling et al. 2023)<sup>203</sup>. After 1h incubation the viral inoculum was removed, cells were washed with pbs and treated with different concentrations of compound MP6. After 48 hours the supernatants were collected for quantification of the viral RNA copy number. Cell media was also collected from treated but not infected controls and untreated but infected controls.

The viral RNA was extracted from the collected samples using the Direct-zol™-96 RNA kit in according to the manufacturer's protocol (Zymo Research, USA) and quantified by RT-qPCR using the SuperScript III OneStep RT-PCR System with Platinum Taq DNA Polymerase kit (Invitrogen, Thermo Fisher Scientific, Waltham, MA). The primers' and probe's sequences used to perform the RT-qPCR were taken from Corman et al. 2020<sup>204</sup>.

## CPE-based antiviral assay – paper IV

Calu-3 cells were seeded one day prior to the assay at a final density of 20.000 cells/well in 96-well plates. After overnight incubation cells were pretreated with the p-glycoprotein inhibitor CP-100356 (MedChemExpress, HY-108347) at a final concentration of 4μM for 2h. After 2h the cell media was discarded, cells were washed with pbs and infected with 200 plaque forming units (~ MOI 0.01) of SARS-CoV-2 (Swedish isolate from Ling et al. 2023)<sup>203</sup>.

The virus inoculum was discarded after 1h incubation, cells were washed with pbs and treated with different concentrations of MP6 and CP-100356 again at a final concentration of 4μM. After 48h the cell media was removed and replaced with fresh cell media. Cells viability was measured performing an MTT assay. Treated but not infected and untreated but infected controls were also included.

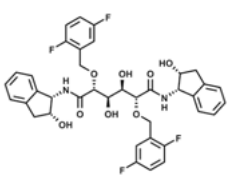
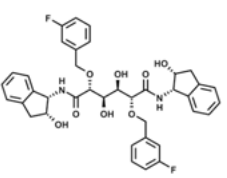
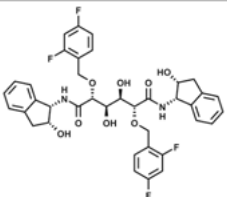
# Results and discussion

## Identification of protease inhibitors against flaviviruses

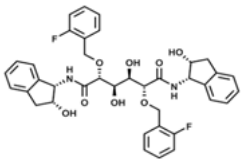
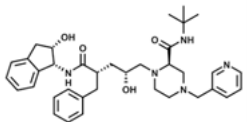
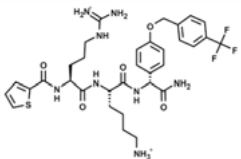
### Identification of active ZIKV protease inhibitor by *in silico* molecular docking and MD simulations (paper I)

Our first study aimed to identify ZIKV NS2B-NS3 protease inhibitors. As described in the introduction, ZIKV can rapidly spread and emerge in new areas of the world. Antivirals against ZIKV would be extremely valuable in preventing and reducing the most severe manifestation of ZIKV infection during future outbreaks that could arise in areas like the south of Europe where the population is still naïve and the mosquito-vector of ZIKV *Aedes albopictus* is already established<sup>61</sup>. In paper I we reported the unexpected identification of the HIV protease inhibitor (PI) “**9b**” with an *in vitro* activity against ZIKV NS2B-NS3 protease. Within this first study we also established all relevant *in silico* and *in vitro* techniques for the identification and testing of compounds, comprising cell-based techniques. In this regard, ZIKV has the advantage of being a BSL-2 pathogen allowing for a faster development of *in vitro* techniques that can be later adapted to other flaviviruses of interest such as e.g. DENV, WNV or TBEV that all require BSL-3 facilities. The PI **9b** was identified by *in silico* screening of a library of 6265 known PIs collected from the MEROPS small-molecule inhibitor database<sup>187</sup> and from the PubChem database<sup>188</sup>. The *in silico*-screening was carried out by consensus molecular docking<sup>205</sup> using AutoDock Vina v1.12<sup>190</sup> and iGEMDOCK v2.1<sup>189</sup>. Both programs placed five HIV protease inhibitors among the top 25 best scoring compounds (Table 2). Interestingly, these HIV inhibitors had a similar score to compound **86**<sup>124</sup>, a known peptide-based pan-flavivirus protease inhibitor (Table 2) without having positively charged groups able to interact with aspartate residues Asp75, Asp83 or Asp129 located in the binding site of ZIKV NS2B-NS3 protease. Molecular dynamics simulations were performed using Gromacs v5.1.1<sup>194</sup> to allow ZIKV protease (PDB ID 5LC0) to relax and dynamically interact for 40 ns with the five PIs as well as **86** that was again used as positive control (binding poses generated by Vina were used to this purpose). While compounds **9e** and **indinavir** dissociated from ZIKV protease during the MD simulations and were not considered for further analysis, compounds **9a**, **9b** and **9f** stably interacted with ZIKV protease during the MD simulations.

**Table 1:** Potential ZIKV protease inhibitors identified by in silico screening.

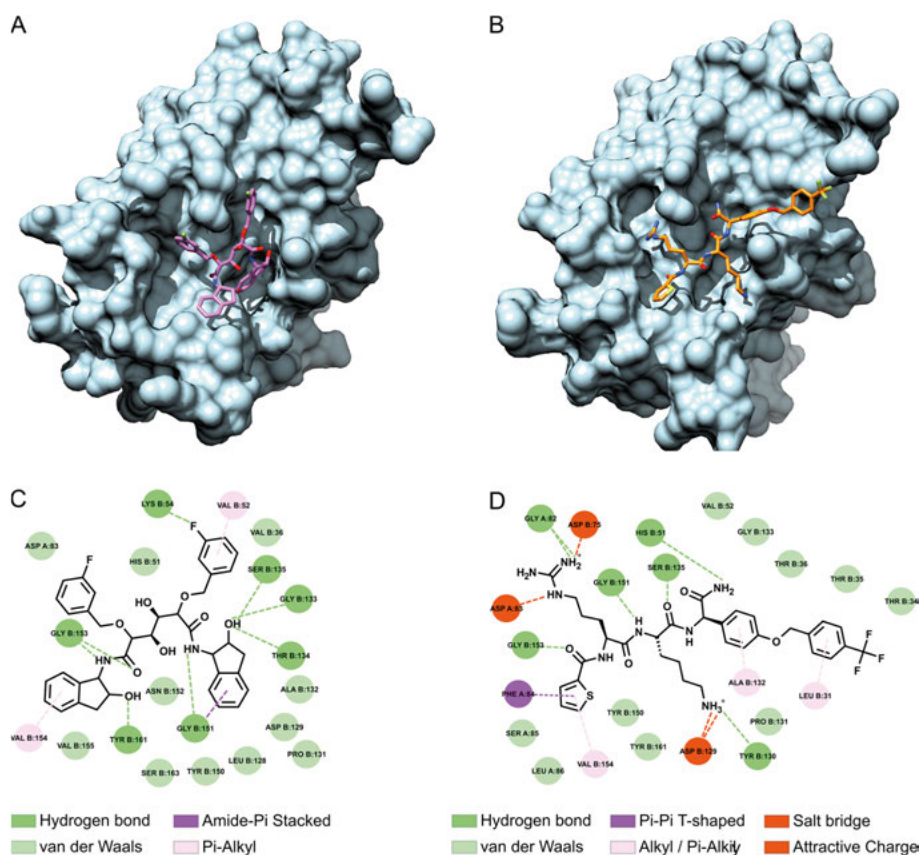
		
Compound 9f <sup>a</sup>	Compound 9b <sup>a</sup>	Compound 9c <sup>a</sup>
Pubchem ID: 449117	Pubchem ID: 449114	Pubchem ID: 449115
Vina score: -9.3 kcal/mol	Vina score: -9.2 kcal/mol	Vina score: -9.1 kcal/mol
iGEMDOCK score: -139,5 kcal/mol	iGEMDOCK score: -119,1 kcal/mol	iGEMDOCK score: -148,3 kcal/mol

		
Compound 9a <sup>a</sup>	Indinavir <sup>b</sup>	Compound 86 <sup>c</sup> (positive control)
Pubchem ID: 445306	Pubchem ID: 5484730	Pubchem ID: not available
Vina score: -8.7 kcal/mol	Vina score: -8.6 kcal/mol	Vina score: -7.4 kcal/mol
iGEMDOCK score: -124.1 kcal/mol	iGEMDOCK score: -149,3 kcal/mol	iGEMDOCK score: 148,2 kcal/mol

(<sup>a</sup>Pyring et al.,2001<sup>206</sup>. <sup>b</sup>Lv et al.,2015<sup>207</sup>, reference 13. <sup>c</sup>Behnam et al.,2015<sup>124</sup>). Adapted from Table 1 of paper I.

Compound **9b** had the most stable conformation over time with an average root mean square deviation (RMSD) of the atomic positions of  $0.22 \pm 0.03$  nm. Given that the conformation of **9b** bound ZIKV protease did not undergo major rearrangement during the MD simulations, we selected **9b** as the best candidate for further analyses. Relevant conformations of compound **9b** and **86** were identified by cluster analyses of the pooled trajectories from the MD simulations and analyzed to identify possible interactions with ZIKV NS2B-NS3 protease (Figure 8). Both compounds were predicted to interact through hydrogen bonds with residues Gly151, Gly153 and Ser135 that is part of the enzyme catalytic triad. The activity of Compound **9b** was tested *in vitro* against ZIKV recombinant protease (bZiPro construct<sup>122</sup>) using a FRET-based enzymatic assay<sup>208</sup>. **Indinavir** and **86** were also tested as negative and positive controls, respectively. As predicted by molecular docking and MD simulations **9b**, but not **indinavir** (data not shown), was active against ZIKV NS2B-NS3 protease (Figure 9). However, when comparing **9b** and **86**, it is evident that the predicted binding affinities (Table 1) poorly correlated with the calculated IC<sub>50</sub>. In fact, Vina estimated a higher binding free energy for **9b** (-9.2 kcal/mol) as compared to **86** (-7.4 kcal/mol) despite **9b** having an IC<sub>50</sub> nearly ninety times higher than **86** (Figure 4).



**Figure 8: Binding poses of compounds **9b** and **86** and possible interactions with ZIKV protease.** Binding poses of ZIKV NS2B-NS3 protease in complex with compound **9b** (A) and **86** (B) from cluster analyses of trajectories from MD simulations. The interactions between the compounds and ZIKV protease, predicted using Discovery Studio v16.1.0.15350 (Dassault Systèmes BIOVIA, San Diego) are shown in (C) and (D). Adapted from Figure 3 of paper I.

To improve the scoring and ranking of the screened compounds using the *in silico* protocol set up in this study, we evaluated the linear interaction energy method (LIE) in combination with MD simulations performed with Q6<sup>197</sup>. The LIE method has the advantage over molecular docking of estimating the binding free energy from multiple binding poses sampled from MD simulations. The estimated binding free energy of **9b** and **86** in complex to ZIKV crystal structure protease (PDBID 5LC0<sup>192</sup>) were -2.29 and -11.62 (kcal/mol) respectively. Since the ZIKV 5LC0 structure was co-crystallized with a covalent peptidomimetic inhibitor, we also applied the LIE method using the apo structure of ZIKV protease (PDBID 5GPI<sup>116</sup>). The free binding energy of the compounds in complex with ZIKV 5GPI structure was -1.45 kcal/mol for **9b** and -4.51 kcal/mol for **86**. The free binding energy of compounds **86** was correctly estimated to be higher than **9b** regardless of the ZIKV protease crystal

structure that was used. Overall, these results better correlated with the compounds activity measured *in vitro* and the LIE method improved the ranking and prediction of the binding affinity of the compounds.

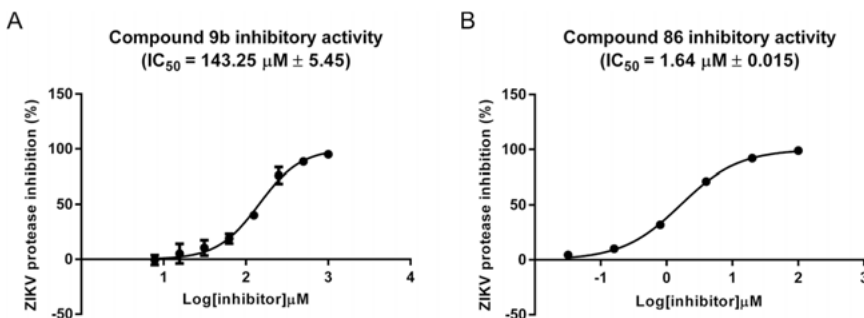


**Figure 9: *In vitro* activity of compounds 9b and 86.** Dose-response curves of the compounds 9b (A) and 86 (B) tested against recombinant ZIKV protease. The average IC<sub>50</sub> values from two independent experiments, each performed with triplicate, are reported with standard errors. Adapted from Figure 4 of paper I.

## Homology modeling of TBEV NS2B-NS3 protease (paper II)

TBEV cases have been increasing in Sweden during the past 20 years<sup>209</sup> and the highest number of infections was reported in 2021 with 534 infections (Public Health agency of Sweden<sup>108</sup>), despite an increase in the number of vaccine doses administered. Currently, no antiviral options are available against TBEV, nor any TBEV NS2B-NS3 protease inhibitor was reported in the literature prior to this study. Moreover, the structure of TBEV NS2B-NS3 protease has not been resolved by x-ray crystallography yet. In this study we have modeled the protease of TBEV *in silico* and used the results to predict the activity of a known pan-flavivirus protease inhibitor active against DENV, WNV and ZIKV.

The preliminary analyses of TBEV NS2B and NS3 amino acid sequences revealed that TBEV protease is conserved among the three subtypes with higher sequence identity between the Siberian and Far-Eastern subtypes (96.33%) and the lowest sequence identity between the European and Siberian subtypes (94%). For comparison, the highest amino acid sequence identity of DENV NS3 proteases among the four serotypes is 74%, observed between DENV type 1 (DENV-1) and type 2 (DENV-2)<sup>210</sup>. While compounds active against the protease of one DENV serotype are usually less potent against the others, compounds with pan-serotype activity have been reported<sup>211–213</sup>. Therefore, we concluded that a possible protease inhibitor active against one TBEV subtype would be active also against the other two and decided to model the NS2B-NS3 protease of the TBEV European subtype.

The structure of the TBEV NS2B-NS3 protease (European subtype, sequence accession number: KF991106.<sup>214</sup>) was folded by homology modeling

<sup>215</sup> using the crystal structures of DENV (PDB ID 3U1I<sup>111</sup>), WNV (PDB ID 5IDK<sup>126</sup>) and ZIKV (PDB ID 5GPI<sup>116</sup>) as template. These were the only NS2B-NS3 crystal structure available in the close and active conformation. The produced model was compared to DENV, WNV and ZIKV NS2B-NS3 protease structures used as templates (Figure 10). The binding site of TBEV NS2B-NS3 presented negatively charged S2 and S1 pockets (Figure 5B) as expected given that the virus protease recognize and cleaves sequence with positively charged amino acid before the cleavage site in position P2-P1 and often also in P3 and P4<sup>114</sup>. The size of TBEV NS2B-NS3 protease (1291 Å<sup>3</sup>) was also comparable to the binding sites of DENV (1191 Å<sup>3</sup>), WNV (1141 Å<sup>3</sup>) and (1184 Å<sup>3</sup>).

### *In silico* modeling of TBEV protease in complex with a known pan-flavivirus protease inhibitor (paper II)

Given the similarities between the binding sites we speculated that the positively charged compound **86**, proven to be active against DENV<sup>124</sup>, WNV<sup>124</sup> and ZIKV<sup>216,217</sup>, would also fit and bind TBEV NS2B-NS3 protease thus inhibiting its activity. We therefore proceeded proving our hypothesis by molecular docking followed by MD simulations as described in our previous publication on ZIKV<sup>216</sup>. Compound **86** bound and interacted with the TBEV NS2B-NS3 protease binding site similarly to DENV, WNV and ZIKV NS2B-NS3 proteases (Figure 11). In the binding poses selected from molecular docking and cluster analyses of MD simulation trajectories, the side chains of compound **86** arginine and lysine residues are positioned in the S2 and S1 pocket where they interact with the negatively charged ASP75 and Asp129. The N-terminal thiophene cap locates in the S3 subsite and the C-terminal group extends over the S1' subsite resembling the positioning of the P3 proline and P2' arginine of aprotinin in complex with WNV NS2B-NS3 protease (paper II, supplementary Figure 2). The free binding energy of **86** in complex with TBEV NS2B-NS3 protease as well as DENV, WNV and ZIKV were calculated using the LIE method and compared. DENV and WNV had the lowest predicted free binding energy followed by TBEV and ZIKV that had the highest predicted free binding energy (Table 2). Interestingly, the reported *in vitro* activity of compound **86** against DENV (IC<sub>50</sub> = 0.028 µM), WNV (IC<sub>50</sub> = 0.117) and ZIKV (IC<sub>50</sub> = 1.64 µM) correlated with the predicted free binding energies. The fact that DENV had the best reported IC<sub>50</sub>, yet second best estimated free binding energy could be explained by the fact that *in vitro* testing was performed with DENV-2 protease while *in silico* modeling was performed with DENV-3 protease (no crystal structure for DENV-2 serotype protease is currently available). Given that TBEV free binding energy was lower (i.e. better) than that of ZIKV, these results suggested that compound **86** had potentially higher *in vitro* inhibitory activity against TBEV than ZIKV.

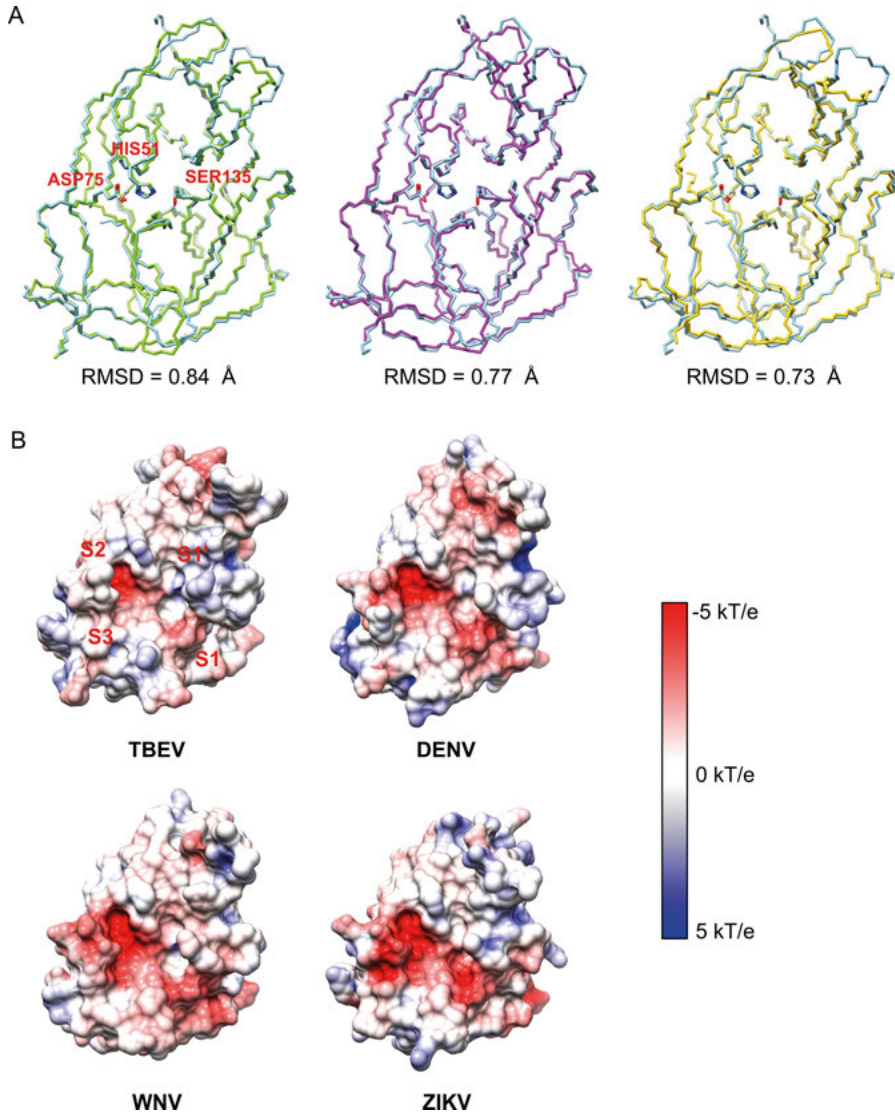
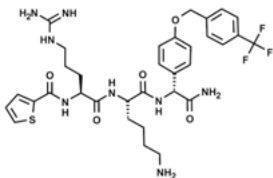


**Figure 10: Comparison of the modeled TBEV NS2B-NS3 protease with DENV, WNV and ZIKV NS2B-NS3 proteases.** (A) TBEV protease (cyan) aligned with DENV (green), WNV (purple) and ZIKV (yellow) proteases. RMSD of the protease's backbones are shown as indicator of structural similarity. (B) Electrostatic surface potential of TBEV, DENV (PDBID 3U1I), WNV (PDBID 5IDK) and ZIKV (PDBID 5GPI) proteases calculated with Delphi<sup>218</sup>. Adapted from Figure 1 of paper II.

**Table 2:** *in silico* estimated binding affinities (kcal/mol  $\pm$  S.E.M) of Compound **86**



Compounds <b>86</b>	
DENV	Vina score: -8.1 LIE binding affinity: $-13.57 \pm 0.53$ ( $IC_{50} = 0.028 \mu M$ ) <sup>a</sup>
WNV	Vina score: -8.7 LIE binding affinity: $-15.94 \pm 1.57$ ( $IC_{50} = 0.117 \mu M$ ) <sup>a</sup>
ZIKV	Vina score: -8.2 LIE binding affinity: $-5.98 \pm 2.21$ ( $IC_{50} = 1.64 \mu M$ ) <sup>b</sup>
TBEV	Vina score: -7.8 LIE binding affinity: $-6.91 \pm 0.98$

<sup>a</sup>(Behnam et al., 2015)<sup>124</sup>, <sup>b</sup>(Akaberi et al. 2020<sup>216</sup>, Kuiper et al., 2017<sup>217</sup>). Adapted from Table 3 of paper II.

## Production of recombinant TBEV protease and enzyme's kinetics (paper II)

To test the predicted inhibitory activity of compound **86**, we expressed and purified the TBEV NS2B-NS3 protease using a construct previously reported by Kurz et al.<sup>219</sup> In this construct NS2B and NS3 are connected by a G4SG4 artificial linker with a cleavage site (K↓EERM) at NS2B C-terminus that allows the protease to self-cleave and assume the unlinked mature form if correctly folded and active. The activity and kinetic parameters of the recombinant protease were measured using the commercially available BZ-Nle-Lys-Arg-Arg-AMC substrate (Bachem Holding AG, Switzerland). The protease was active and its  $K_m$  was similar to other flaviviruses for the substrate<sup>117,118,220</sup>, however the enzymatic activity was very low ( $k_{cat} = 0.0039$  s<sup>-1</sup>).

## Compound **86** and similar peptidomimetics inhibits TBEV protease *in vitro* (paper II)

We finally confirmed the inhibitory activity of compound **86** and other similar peptide-based compounds against TBEV NS2B-NS3 recombinant protease using a FRET-based enzymatic assay (Figure 8). Compounds were also tested against ZIKV for comparison. All compounds were active against TBEV protease, compounds **86** and **104** had similar activity with an  $IC_{50}$  of 0.92 and 0.97  $\mu M$  respectively, while compound **6C** was the less active with an  $IC_{50}$  of 72  $\mu M$ . Given that the only difference between compound **104** and **6C** was the substitution of **104**'s P1 lysine (shown in orange in Figure 12) with an





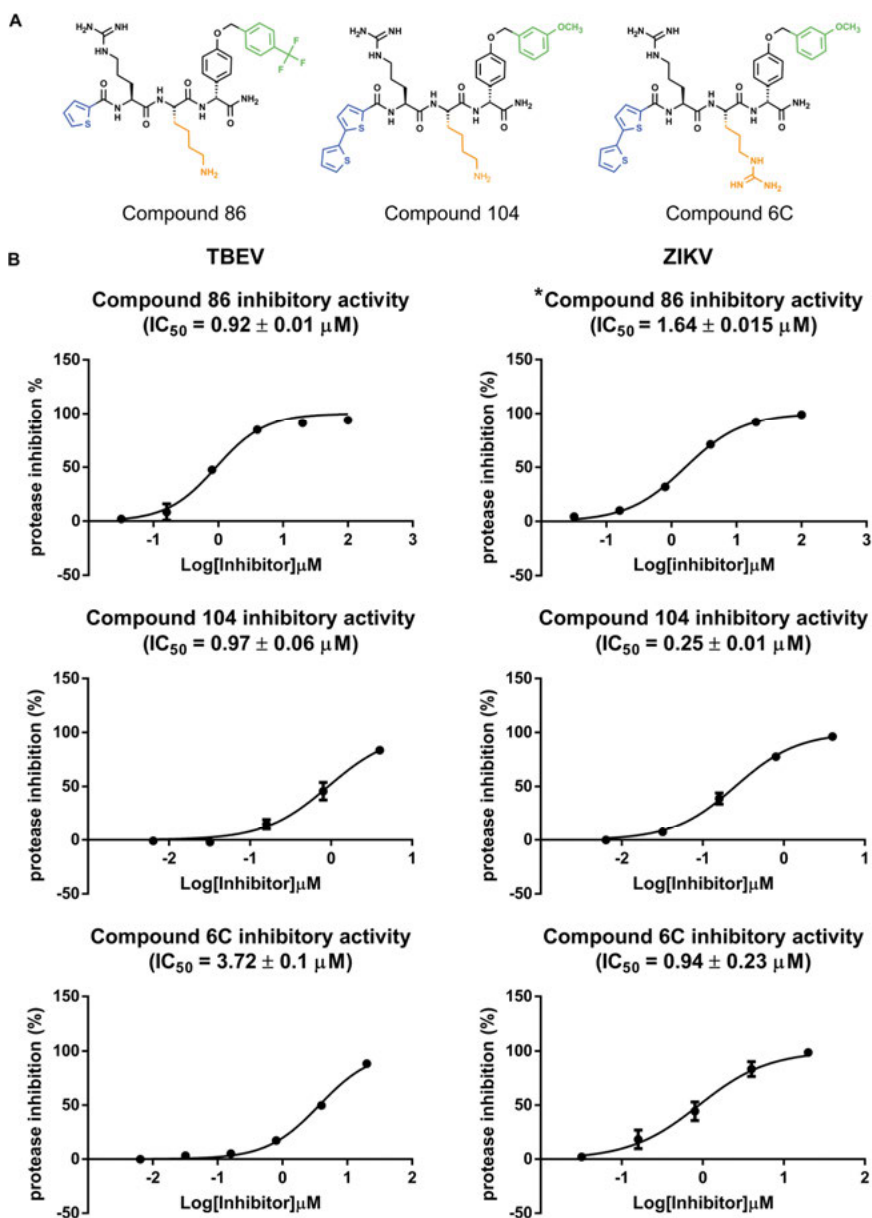


**Figure 12: Inhibitory activity of peptidomimetics compounds against TBEV and ZIKV proteases.** Compounds **86**, **104** and **6C** exhibit inhibitory activity against TBEV and ZIKV proteases in an *in vitro* enzymatic assay. (A) Structures of Compounds **86**, **104** and **6C** with different N-terminal cap, P1 residue and C-terminal residue's benzyl ether shown in blue, orange and green, respectively. (B) Dose response curves of Compounds **86**, **104** and **6C** tested against TBEV and ZIKV proteases. Values represent mean  $\pm$  S.E.M from two independent experiments (each performed as technical triplicates). Adapted from Figure 5 of paper II.

# Identification of protease inhibitors against coronaviruses

## The NO donor SNAP inhibits SARS-CoV-2 replication *in vitro* (paper III)

Nitric oxide (NO) releasing compounds like SNAP (S-Nitroso-N-acetyl-DL-penicillamine) have been proven to inhibit SARS-CoV-1 replication *in vitro*<sup>221,222</sup>, however, no information were available on the possible antiviral effect and mechanism of action of NO against SARS-CoV-2 when the outbreak started. In 2020, we tested the *in vitro* antiviral activity of NO against SARS-CoV-2 and found that SNAP also inhibited SARS-CoV-2 replication possibly interfering with its main protease activity (Study III). Vero E6 cells were treated with either SNAP or NAP (a variant of SNAP that does not release NO) every four hours for 36 hours while viral replication was measured every four hours for 72 hours (Figure 13). SNAP had a dose dependent inhibitory effect but never completely suppressed SARS-CoV-2 replication.

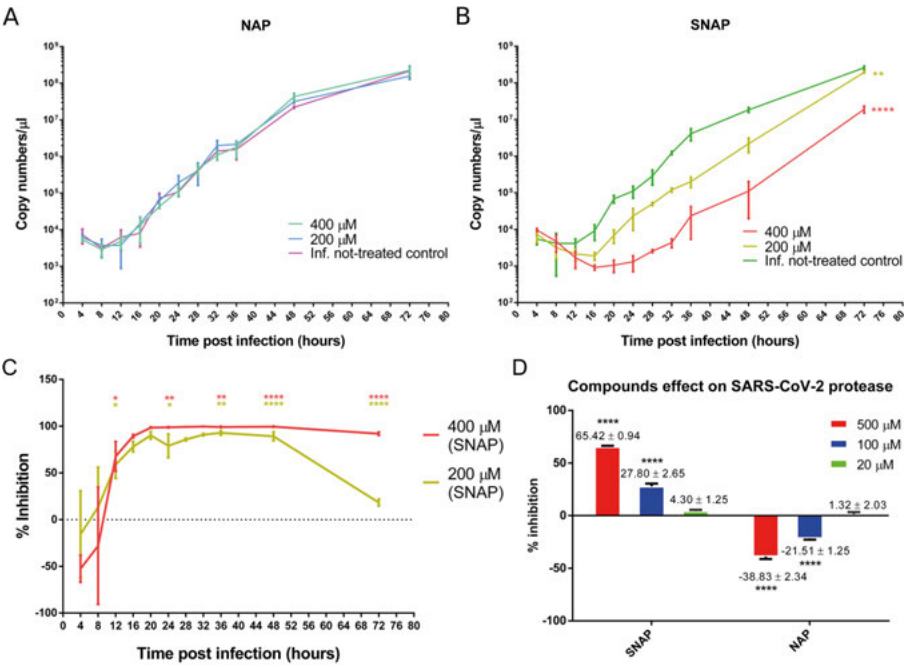


**Figure 13: SNAP inhibitory effect on SARS-CoV-2 replication and M<sup>pro</sup> enzymatic activity.** (A) effect of NAP and (B) SNAP treatment on SARS-CoV-2 replication kinetics in Vero-E6 cells. (C) NAP and SNAP inhibitory effect plotted as percentage of the viral replication reduction over time. (D) NAP and SNAP effect on the enzymatic activity of SARS-CoV-2 M<sup>pro</sup>. Statistical significance is reported as \*\*p < 0.001, \*\*\*\*p < 0.0001 (comparison with the controls).

At 36 hours post infection (hpi), when cells were retreated for the last time, SARS-CoV-2 replication was reduced by 99.42% ( $\pm 0.44$  SD) and 95.07% ( $\pm 1.58$  SD) when the infected cells were treated with 400  $\mu$ M and 200  $\mu$ M of SNAP, respectively. However, the inhibition of the viral replication decreased to 25.10% ( $\pm 3.37$  SD) in infected cells treated with 200  $\mu$ M at 72 hpi (36 hours after the last retreatment), while it was still above 90% in infected cells treated with 400 of SNAP (Figure 13). The reduction in SARS-CoV-2 replication was associated with an observable reduction in cytopathic effect (CPE) development in infected and treated cells (Figure 3, paper III). Ultimately, we tested the possible inhibitory effect of SNAP on the activity of SARS-CoV-2 3CL protease. Saura and co-workers have previously reported the *in vitro* inhibition of Coxsackievirus B3 3C cysteine protease activity mediated by SNAP<sup>223</sup>. Since SARS-CoV-2 3CL protease is also a cysteine protease, we speculated that SNAP could have been able to inhibit SARS-CoV-2 protease by transnitration (direct transfer of a nitrosonium ion ( $\text{NO}^+$ )) of the catalytic Cys145. SARS-CoV-2 3CL protease was incubated with different concentrations of SNAP or NAP for 10 minutes before the addition of a FRET substrate to start the proteolytic reaction. SNAP inhibited SARS-CoV-2 3CL protease activity, while NAP act as a reducing agent increasing the protease activity (**Figure 11**).

## Identification of a novel class of potent peptidomimetics inhibitors of SARS-CoV-2 main protease (paper IV)

DNA-encoded chemical libraries (DECL) are large collection of combinatorial compounds tagged with a unique bar code that allows the identification of each single molecule<sup>224</sup>. Affinity screening of DECL allows the ultra-rapid and cost-efficient exploration of large portion of chemical space that cannot be accomplished with any other *in vitro* drug discovery tool in the same amount of time. Moreover, screening of DECL can be performed with basic laboratory equipment and has the advantage over other techniques like high-throughput screening of not requiring automation or dedicated infrastructures. In this study we identified novel and potent inhibitors of SARS-CoV-2 protease through affinity screening of the DELopen (WuXi AppTec) library composed of 4.2 billion unique compounds from 27 different libraries. Binders were identified by three rounds of affinity selection against recombinant avitagged SARS-CoV-2 M<sup>pro</sup>. To possibly differentiate between compounds that binds to M<sup>pro</sup> active site versus compounds that binds to allosteric sites, the selection process was also performed in presence of compounds X77 and GC376 that are known to bind to SARS-CoV-2 M<sup>pro</sup>. After three rounds of selection four enriched binders (Table 3) with high affinity for M<sup>pro</sup> were identified, synthesized off-DNA (i.e. without the DNA tag) and tested against recombinant SARS-CoV-2 M<sup>pro</sup> using a FRET-based enzymatic assay. Three out of four compounds were active with IC<sub>50</sub> lower than 200nM. The compounds **SLL11** and **SLL12** were the two most potent compounds with IC<sub>50</sub>

equal to 30 and 53 nM respectively. Interestingly, these two compounds were also the most enriched during selection, while the least enriched compounds, **SLL08**, was not active. All active compounds had not off-target activity towards human Cathepsin S (also a cysteine protease) when tested at concentrations up to 50  $\mu$ M.

**Table 3:** List of compounds selected from DECL and relative in vitro activity.

Comp.	Enrichment score <sup>a</sup>				IC <sub>50</sub> ( $\mu$ M)		
	Mpro	Mpro +X77	Mpro +GC376	Beads only	Mpro		Cathepsin S
SLL07	135654	0	0	0	0.14	0.082	> 50
SLL08	11444	0	676	0	> 50	> 50	> 50
SLL11	515485	20997	206982	0	0.030	0.029	> 50
SLL12	488354	0	0	0	0.053	0.056	> 50

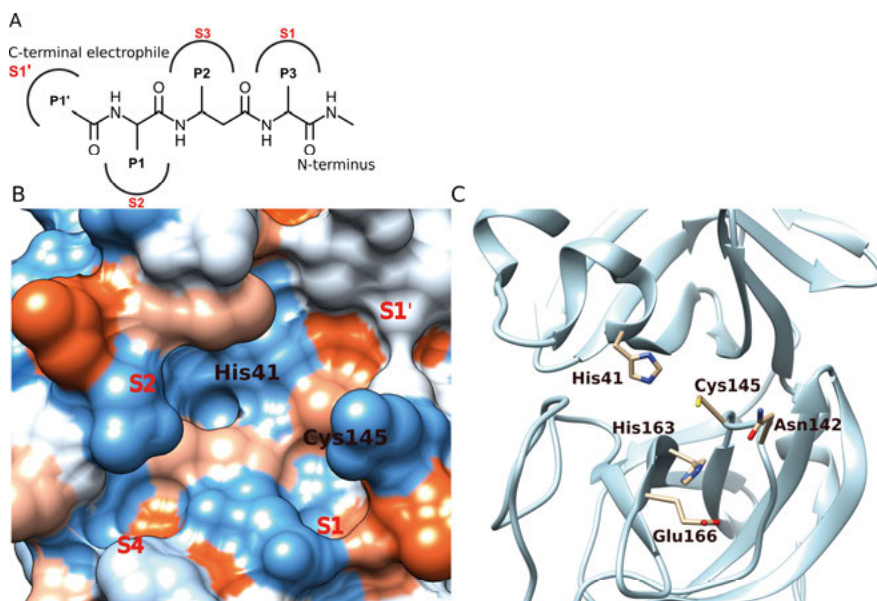
<sup>a</sup>The enrichment score quantify how abundant a compound was after selection, e.g. a compound with enrichment score = 100 was 100 times more abundant than average

The binding poses SLL11 and SLL12 in complex with Mpro were identified by x-ray crystallography, the structures will not be disclosed due to pending patent filing. Both compounds were confirmed to bind to SARS-CoV-2 M<sup>pro</sup> binding site forming similar interactions. The general structure of both **SLL11** and **SLL12** is shown in Figure 14, both compounds had a P1' electrophilic group that formed a covalent bond with Cys145 of the enzyme catalytic dyad. The remaining three groups in position P1, P2 and P3 were located in the S2, S4 and S1 subsites of M<sup>pro</sup> binding site. Hydrogen bonds were formed between the P3 group and the His163 sidechain in S1, between the compounds and Glu166 backbones and between the compounds N-terminal amine of SLL11 and Asn142 side chain.

## Structure-activity relationship (SAR) study (paper IV)

Several analogs of **SLL11**, the most potent compounds selected, were synthesized to perform a structure-activity relationship (SAR) study. The compound **MP6** was synthesized from **SLL11** by substituting the methylamine N-terminus with a carboxylic group to possibly improve solubility (Table 4) and was used as comparison for all the other analogues synthesized. **MP6** and its variants were tested at a concentration of 1  $\mu$ M and compounds inhibiting SARS-CoV-2 M<sup>pro</sup> by 80% or more where retested to calculate an IC<sub>50</sub>. Removing the groups in P3 or P2 reduce inhibitory activity from 97% (**MP6**) to 2.2% (**MP2**) and 8.1% (**MP4**). Substituting the P3 group with one that cannot form a hydrogen bond with His163 (**MP7**, **MP13**) or the P1' electrophilic group with a less reactive one (**MP5**) also almost completely abolished the compounds inhibitory activity. No loss of activity was observed when substituting the P1' electrophilic group with a highly reactive aldehyde group (**MP9**).

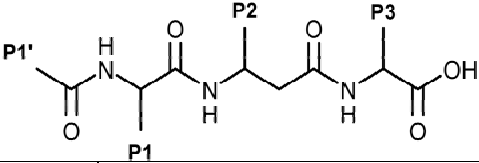
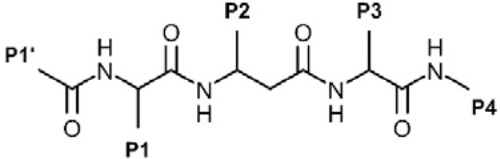
Analogues with different hydrophobic groups in P1 (**MP3**, **MP16** and **MP17**) were active with  $IC_{50}$  ranging from 69 to 139 nM. Adding a fifth group at the N-terminus of MP6 was also well tolerated and the resulting compounds had  $IC_{50}$  ranging from 33 to 106 nM. Overall, these results suggested that the compounds selected by affinity were already well optimized and confirmed that potent inhibitors can be directly identified from screening large portion of chemical space without the need for intensive medicinal chemistry.



**Figure 14: Compounds structure and binding modes.** (A) General structure of SLL11 and SLL12. The surface of SARS-CoV-2 Mpro (PDBID 7PFM) active site colored based on amino acids hydrophobicity (blue hydrophilic, red hydrophobic). The four main subsites are labeled in red and His41 and Cys145 of the catalytic dyad are also shown. (C) Residues in the M<sup>pro</sup> binding site found interacting with SLL11 and SLL12 in crystallographic binding poses.

The effect of the nirmatrelvir resistant variant E166V on the inhibitory activity of MP9 (variant of MP6 having a P1' aldehyde group) against M<sup>pro</sup> was tested and compared to nirmatrelvir. Both compounds had  $IC_{50}$  in the low nanomolar range (Figure 15A) against WT M<sup>pro</sup>. The variant E166V caused a 523-fold increase in MP9's  $IC_{50}$  and a 473-fold increase in nirmatrelvir's  $IC_{50}$  against M<sup>pro</sup>, respectively. E166V was shown to induce resistance against nirmatrelvir by disrupting key interaction at the S1 site through steric hindrance that ultimately misplace the nitrile warhead reducing the efficiency of interaction with the Cys145 of the catalytic dyad<sup>225,226</sup>. Similar dynamics might be involved in reducing the activity of MP9 against M<sup>pro</sup> carrying the E166V variant.

**Table 4:** Inhibitory activity of compounds used in the SAR study.

<b>Backbone structure</b> 			
Compound	Variant	M <sup>pro</sup> Inhibition % <sup>a</sup> (Comp. conc. 1μM)	IC <sub>50</sub> ± SEM (μM) <sup>b</sup>
MP6	None (reference)	97% ± 4.9 SD	0.025 ± 0.001
MP2	Missing P3 residue (whole residue)	2.2%	n.d.
MP4	Missing P2 side group	8.1%	n.d.
MP5	less reactive P1' electrophile	17.8%	n.d.
MP7	Different P3	30.4%	n.d.
MP9	Different P1' group (aldehyde)	100%	0.024 ± 0.0004
MP13	Different P3	38% ± 16.2 SD	n.d.
MP16	Different P1	95.7% ± 1.3 SD	0.071 ± 0.007
MP17	Different P1	90.7% ± 1.6 SD	0.069 ± 0.004
MP22	Electrophilic P1' group	18.2%	n.d.
MP3	Different P1	86.6% ± 1.1 SD	0.139 ± 0.049
<b>Backbone structure</b> 			
Compound	Variant	M <sup>pro</sup> Inhibition % (Comp. conc. 1μM)	IC <sub>50</sub> ± SEM (μM)
MP12	Additional P4 group	96.5% ± 4.5 SD	0.106 ± 7 <sup>c</sup>
MP18	Additional P4 group	94.2% ± 5.7 SD	0.047 ± 0.006
MP19	Additional P4 group	98.2% ± 2.6 SD	0.045 ± 0.009
MP20	Additional P4 group	66.8%	n.d.
MP21	Additional P4 group	94.7% ± 3.4	0.033 ± 0.003

Continues in the next page.

<sup>a</sup> Compounds were tested at a concentration of 1  $\mu\text{M}$  in triplicates ( $n = 3$  replicates). Average inhibition of  $\text{M}^{\text{pro}} \pm$  standard deviation (SD) is shown only for compounds that were tested in two independent experiments.

<sup>b</sup> Average  $\text{IC}_{50}$  and standard error of the mean (SEM) were calculated from two independent experiments where each compound's concentration was tested in triplicates ( $n = 3$  replicates).

<sup>c</sup> The  $\text{IC}_{50}$  of compounds MP12 was determined from a single experiment where each compound's concentration was tested in triplicates ( $n = 3$  replicates), standard deviation (SD) is reported instead of SEM.

## Antiviral activity of MP6 in Calu-3 and Caco-2 cell lines (paper IV)

The antiviral activity of compound MP6 was tested in cell-based assays. MP6 inhibited SARS-CoV-2 replication in Caco-2 cells and CPE development induced by SARS-CoV-2 in infected Calu-3 with  $\text{EC}_{50} = 2.3 \pm 1.1 \mu\text{M}$  (Figure 15B and C). The addition of the p-glycoprotein (P-gp) inhibitor CP-100356, previously used to test nirmatrelvir in cell-based assays<sup>177,227,228</sup>, was indispensable for the activity of MP6 in Calu-3 cells but not in Caco-2 cells.

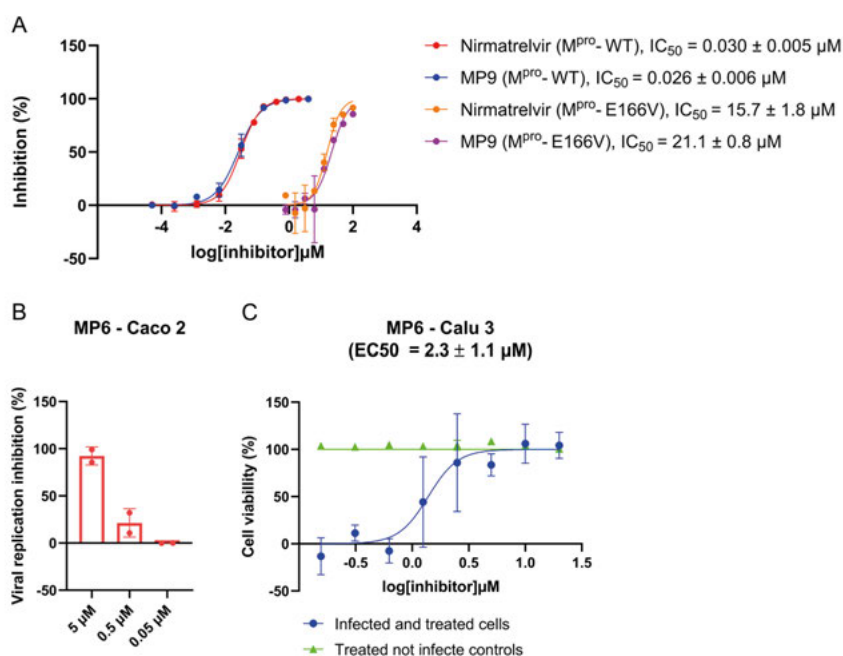


**Figure 15: MP9 inhibitory activity against resistant  $\text{M}^{\text{pro}}$  and MP6 antiviral activity in cell-based assays.** (A) Inhibitory activity of MP9 and nirmatrelvir against recombinant  $\text{M}^{\text{pro}}$  WT and E166V variant. (B) MP6 inhibitory activity against SARS-CoV-2 replication in Caco-2. (C) MP6 inhibition on CPE development in infected Calu-3 cells.



## Conclusions and future prospectives

The flavivirus genus (Flaviviridae family) and betacoronavirus genus (Coronavirinae family) contain several important human pathogens such as Dengue (DENV), West Nile (WNV), Zika (ZIKV), tick-borne encephalitis (TBEV), SARS-CoV, MERS-CoV, and SARS-CoV-2 viruses. Given the potential of both flavivirus and betacoronaviruses to emerge and spread, antiviral options for the prevention and treatment of flavivirus and coronavirus infections are urgently needed.

In this thesis we reported the identification of protease inhibitors against flaviviruses and betacoronaviruses. In the first paper we report unexpected identification of an HIV-1 protease inhibitor “**9b**” with an *in vitro* activity against ZIKV NS2B-NS3 protease. Although **9b** only had a modest activity against ZIKV protease ( $IC_{50} = 143.25 \pm 5.45 \mu M$ ), the combination of docking and molecular dynamics simulations employed in the study proved to be able to correctly identify active compounds. The addition of free binding energy estimations using the linear interaction energy method further improved the predictive performance of the *in silico* techniques we used, and should be used in future studies to help discriminating between less and more potent compounds. In the second paper we reported the first protease inhibitors active against TBEV. These compounds can be used as reference to set up *in vitro* enzymatic and possibly also cell-based assays for testing of potential TBEV protease inhibitors. The data presented in the second paper also provides new knowledge for the further development of TBEV and more importantly pan-flavivirus protease inhibitors. Regarding future prospectives, we have redirected our research efforts on the discovery of protease inhibitors against DENV. Thanks to a new collaboration established with ANYO Labs at the start of 2023, several million compounds have been generated “de novo” and screened *in silico* against DENV type 2 and 3 proteases using a novel drug discovery tool based on artificial intelligence (AI). The knowledge and experience gained during our first two studies has already been proved instrumental and currently we have set up an enzymatic assay that will be soon used to test identified possible DENV protease inhibitors. Once validated and possibly also further trained, this AI-technology could provide the muscle for the identification of potent pan-flavivirus protease inhibitors, which still represent the ultimate goal.

The same is true for coronavirus protease inhibitors. Since I started my PhD in the summer of 2020, several SARS-CoV-2 protease inhibitors have been reported and the race to develop a cure for SARS-CoV-2 was won by Pfizer with the approval of Paxlovid (nirmatrelvir) for clinical use. The future is therefore focused, in my opinion, on the development of better pan-coronavirus inhibitors. In the 21<sup>st</sup> century three coronaviruses have emerged (SARS-CoV, MERS-CoV and SARS-CoV-2) and although there is no telling when the next one will emerge, it is safe to assume that humanity will face another coronavirus outbreak or pandemic in the future. Pan-coronavirus protease inhibitors would provide an early prophylactic tool and cure to protect healthcare workers, reduce early transmissions and fatal infections. In our third paper we evaluated the antiviral activity of nitric oxide (NO) against SARS-CoV-2 and found that SNAP, an NO-releasing compound, was able to reduce viral replication and CPE development in a dose dependent manner. We also observed that SNAP inhibited the activity of SARS-CoV-2 M<sup>pro</sup> using an enzymatic assay. However, SARS-CoV-2 M<sup>pro</sup> still needs to be properly evaluated as a possible target for the antiviral activity of NO using cell-based assays. These experiments are on their way and if they are going to finally establish M<sup>pro</sup> as a possible target for nitrosation, a new class of novel broad-spectrum pan-coronavirus protease inhibitors could be developed.

In our fourth and last study, we have identified potent SARS-CoV-2 protease inhibitors from affinity screening of the DELopen (WuXi AppTec) DNA-encoded chemical library. These compounds need to be evaluated against different coronaviruses to assess their pan-coronavirus activities. The cyclization or substitution of selected residues with D-enantiomers could be attempted to improve metabolic stability, cell permeability and the overall performance of the compounds in cell-based assays.

There is much left to do, but I hope I will keep working and further contribute to the exciting multidisciplinary field of antiviral research.

# Acknowledgments

I would like to start by thanking my supervisors **Johan Lennerstrand** and **Åke Lundkvist**, without you I would not be here writing my PhD thesis.

Dear Johan, you gave me the opportunity to keep working in your lab after I finished my master project, which was the first step that led me to where I am today. I will always be grateful to you for providing me with interesting projects and an environment where I have been encouraged to experiment, find my own way to answer scientific questions and solve problems. See you on the golf course!

Dear Åke, you welcomed me into your group, and gave me the chance to keep pursuing my research interests. I am extremely grateful for the guidance, trust, and freedom I enjoyed while working with you.

I also thank **Josef Järhult** for the support, I really appreciate it.

I have been extremely lucky to meet and work with **Navaneethan Palanisamy**, a great scientist and the most hard working person I know. You introduced me to all the *in silico* techniques I used, and it was while working with you that I co-authored my first publication! I have fond memories of the times you came to visit Johan and me in Uppsala. I consider you a true mentor and a dear friend. I wish you all the happiness and luck in the world.

To our collaborators from the department of medicinal chemistry: **Praveen Chinthakindi**, **Amanda Båhlström**, **Monireh Lati** and in particular **Oscar Verho** and **Anja Sandström**. Thanks, without you I would not have had compounds to test!

Thanks also to **Tomas Nyman** and all other collaborators from PSF for the proteases that I used in my studies, **Martin Moche** for the excellent crystallographic work, **Kristian Sandberg** and DDD for the support and expertise that gave us access to the DECL technology.

**Filip**, unfortunately we met only at the end of yours and my PhD studies, but I hope we will work together in the future. Thank you for listening to me talking about my research like a broken record and for always being available when I had a question about biochemistry. You are a true treasure.

Thanks to all the people at the zoonosis science center and in particular **Tove, Jenny, Patrik, and Anisha**. You have all been very patient and kind to me. **Jiixin**, it was fun to share the old office with you, we had a lot of discussion and laughs. Thanks for helping me every time I went in the BSL3 lab and forgot my cells in the incubator outside!

**Mahmoud**, thanks for all the help, lunches, fikas and of course the mangoes!

And last but not least, a big thank you to my colleague and dearest friend **Janina**. Thanks for every minute we spent together working, discussing, or having fun at work or outside! It is priceless to have someone you can always count on.

I cannot forget to thank my uncle **Shahriar, Louise** and my two lovely cousins **Linnea** and **Malva** for welcoming me to Sweden and always making me feel at home in Lomma.

And finally, thanks to my amazing parents **Cinzia** and **Jamshid** that unconditionally supported me for so many years without ever saying “no” once. I owe you everything I have achieved so far. Dear grandma **Lucia**, thanks for teaching me so many amazing recipes, they all came in handy! Dear sister **Annalisa, Fabrizio** and **Niccolò**, thanks to you too for all the fun video calls, it is always heartwarming to see you all becoming a beautiful family!

## References

1. Bhatt, S. *et al.* The global distribution and burden of dengue. *Nature* **496**, 504–507 (2013).
2. Shepard, D. S., Undurraga, E. A., Halasa, Y. A. & Stanaway, J. D. The global economic burden of dengue: a systematic analysis. *The Lancet Infectious Diseases* **16**, 935–941 (2016).
3. Organization, W. H. Zika virus, microcephaly and Guillain-Barré syndrome situation report. (2016).
4. Frutos, R., Serra-Cobo, J., Pinault, L., Lopez Roig, M. & Devaux, C. A. Emergence of Bat-Related Betacoronaviruses: Hazard and Risks. *Frontiers in Microbiology* **12**, (2021).
5. Teramoto, T., Choi, K. H. & Padmanabhan, R. Flavivirus proteases: The viral Achilles heel to prevent future pandemics. *Antiviral Research* **210**, 105516 (2023).
6. Li, J. *et al.* Structural Basis of Main Proteases of Coronavirus Bound to Drug Candidate PF-07304814. *Journal of Molecular Biology* **434**, 167706 (2022).
7. Chambers, T. J., Hahn, C. S., Galler, R. & Rice, C. M. Flavivirus genome organization, expression, and replication. *Annu Rev Microbiol* **44**, 649–688 (1990).
8. Ishak, R., Tovey, D. G. & Howard, C. R. Morphogenesis of yellow fever virus 17D in infected cell cultures. *J Gen Virol* **69** ( Pt 2), 325–335 (1988).
9. Ng, M. L. & Lau, L. C. Possible involvement of receptors in the entry of Kunjin virus into Vero cells. *Arch Virol* **100**, 199–211 (1988).
10. Chao, L. H., Klein, D. E., Schmidt, A. G., Peña, J. M. & Harrison, S. C. Sequential conformational rearrangements in flavivirus membrane fusion. *eLife* **3**, e04389 (2014).
11. Bressanelli, S. *et al.* Structure of a flavivirus envelope glycoprotein in its low-pH-induced membrane fusion conformation. *EMBO J* **23**, 728–738 (2004).
12. Corver, J. *et al.* Membrane fusion activity of tick-borne encephalitis virus and recombinant subviral particles in a liposomal model system. *Virology* **269**, 37–46 (2000).
13. Byk, L. A. *et al.* Dengue Virus Genome Uncoating Requires Ubiquitination. *mBio* **7**, e00804-16 (2016).

14. Garcia-Blanco, M. A., Vasudevan, S. G., Bradrick, S. S. & Nicchitta, C. Flavivirus RNA transactions from viral entry to genome replication. *Antiviral Research* **134**, 244–249 (2016).
15. Nicholls, C. M. R., Sevvana, M. & Kuhn, R. J. Chapter Two - Structure-guided paradigm shifts in flavivirus assembly and maturation mechanisms. in *Advances in Virus Research* (eds. Kielian, M., Mettenleiter, T. C. & Roossinck, M. J.) vol. 108 33–83 (Academic Press, 2020).
16. Chambers, T. J. *et al.* Evidence that the N-terminal domain of nonstructural protein NS3 from yellow fever virus is a serine protease responsible for site-specific cleavages in the viral polyprotein. *Proc Natl Acad Sci USA* **87**, 8898–8902 (1990).
17. Falgout, B., Pethel, M., Zhang, Y. M. & Lai, C. J. Both nonstructural proteins NS2B and NS3 are required for the proteolytic processing of dengue virus nonstructural proteins. *J Virol* **65**, 2467–2475 (1991).
18. Chambers, T. J., Grakoui, A. & Rice, C. M. Processing of the yellow fever virus nonstructural polyprotein: a catalytically active NS3 proteinase domain and NS2B are required for cleavages at dibasic sites. *J Virol* **65**, 6042–6050 (1991).
19. Welsch, S. *et al.* Composition and Three-Dimensional Architecture of the Dengue Virus Replication and Assembly Sites. *Cell Host & Microbe* **5**, 365–375 (2009).
20. Płaszczycza, A. *et al.* A novel interaction between dengue virus nonstructural protein 1 and the NS4A-2K-4B precursor is required for viral RNA replication but not for formation of the membranous replication organelle. *PLOS Pathogens* **15**, e1007736 (2019).
21. Scaturro, P., Cortese, M., Chatel-Chaix, L., Fischl, W. & Bartenschlager, R. Dengue Virus Non-structural Protein 1 Modulates Infectious Particle Production via Interaction with the Structural Proteins. *PLoS Pathog* **11**, e1005277 (2015).
22. Miller, S., Kastner, S., Krijnse-Locker, J., Bühler, S. & Bartenschlager, R. The Non-structural Protein 4A of Dengue Virus Is an Integral Membrane Protein Inducing Membrane Alterations in a 2K-regulated Manner \*. *Journal of Biological Chemistry* **282**, 8873–8882 (2007).
23. Umareddy, I., Chao, A., Sampath, A., Gu, F. & Vasudevan, S. G. Dengue virus NS4B interacts with NS3 and dissociates it from single-stranded RNA. *J Gen Virol* **87**, 2605–2614 (2006).
24. Alvarez, D. E., Lodeiro, M. F., Ludueña, S. J., Pietrasanta, L. I. & Gamarnik, A. V. Long-Range RNA-RNA Interactions Circularize the Dengue Virus Genome. *Journal of Virology* **79**, 6631–6643 (2005).
25. Xie, X. *et al.* Dengue NS2A Protein Orchestrates Virus Assembly. *Cell Host Microbe* **26**, 606-622.e8 (2019).
26. Cortese, M. *et al.* Ultrastructural Characterization of Zika Virus Replication Factories. *Cell Reports* **18**, 2113–2123 (2017).

27. Yu, I.-M. *et al.* Structure of the Immature Dengue Virus at Low pH Primes Proteolytic Maturation. *Science* **319**, 1834–1837 (2008).
28. D’Ortenzio, E. *et al.* Evidence of Sexual Transmission of Zika Virus. *N Engl J Med* **374**, 2195–2198 (2016).
29. Driggers, R. W. *et al.* Zika Virus Infection with Prolonged Maternal Viremia and Fetal Brain Abnormalities. *New England Journal of Medicine* **374**, 2142–2151 (2016).
30. Hudopisk, N. *et al.* Tick-borne Encephalitis Associated with Consumption of Raw Goat Milk, Slovenia, 2012. *Emerg Infect Dis* **19**, 806–808 (2013).
31. Caini, S. *et al.* Tick-borne encephalitis transmitted by unpasteurised cow milk in western Hungary, September to October 2011. *Eurosurveillance* **17**, 20128 (2012).
32. Gresíková, M., Sekeyová, M., Stúpalová, S. & Necas, S. Sheep milk-borne epidemic of tick-borne encephalitis in Slovakia. *Intervirology* **5**, 57–61 (1975).
33. Holzmann, H. *et al.* Tick-borne encephalitis from eating goat cheese in a mountain region of Austria. *Emerg Infect Dis* **15**, 1671–1673 (2009).
34. Woodall, J. P. & Roz, A. Experimental milk-borne transmission of Powassan virus in the goat. *Am J Trop Med Hyg* **26**, 190–192 (1977).
35. Alzahrani, A. G. *et al.* Alkhurma Hemorrhagic Fever in Humans, Najran, Saudi Arabia. *Emerg Infect Dis* **16**, 1882–1888 (2010).
36. Weaver, S. C. & Barrett, A. D. T. Transmission cycles, host range, evolution and emergence of arboviral disease. *Nat Rev Microbiol* **2**, 789–801 (2004).
37. Vasilakis, N. & Weaver, S. C. Flavivirus transmission focusing on Zika. *Current Opinion in Virology* **22**, 30–35 (2017).
38. Gabiane, G., Yen, P.-S. & Failloux, A.-B. Aedes mosquitoes in the emerging threat of urban yellow fever transmission. *Reviews in Medical Virology* **32**, e2333 (2022).
39. Duangkhae, P. *et al.* Interplay between Keratinocytes and Myeloid Cells Drives Dengue Virus Spread in Human Skin. *Journal of Investigative Dermatology* **138**, 618–626 (2018).
40. Hamel, R. *et al.* Biology of Zika Virus Infection in Human Skin Cells. *J Virol* **89**, 8880–8896 (2015).
41. Labuda, M. *et al.* Importance of Localized Skin Infection in Tick-Borne Encephalitis Virus Transmission. *Virology* **219**, 357–366 (1996).
42. Wu, S.-J. L. *et al.* Human skin Langerhans cells are targets of dengue virus infection. *Nat Med* **6**, 816–820 (2000).
43. Wang, K. & Deubel, V. Mice with Different Susceptibility to Japanese Encephalitis Virus Infection Show Selective Neutralizing Antibody Response and Myeloid Cell Infectivity. *PLOS ONE* **6**, e24744 (2011).

44. Johnston, L. J., King, N. J. C. & Halliday, G. M. Langerhans Cells Migrate to Local Lymph Nodes Following Cutaneous Infection with an Arbovirus. *Journal of Investigative Dermatology* **114**, 560–568 (2000).
45. Cerny, D. *et al.* Selective Susceptibility of Human Skin Antigen Presenting Cells to Productive Dengue Virus Infection. *PLOS Pathogens* **10**, e1004548 (2014).
46. Taweechaisupapong, S. *et al.* Langerhans cell density and serological changes following intradermal immunisation of mice with dengue 2 virus. *J Med Microbiol* **45**, 138–145 (1996).
47. Pierson, T. C. & Diamond, M. S. The continued threat of emerging flaviviruses. *Nat Microbiol* **5**, 796–812 (2020).
48. Chitimia-Dobler, L. *et al.* Repeated isolation of tick-borne encephalitis virus from adult Dermacentor reticulatus ticks in an endemic area in Germany. *Parasites & Vectors* **12**, 90 (2019).
49. Pattnaik, P. Kyasanur forest disease: an epidemiological view in India. *Rev Med Virol* **16**, 151–165 (2006).
50. Růžek, D., Yakimenko, V. V., Karan, L. S. & Tkachev, S. E. Omsk haemorrhagic fever. *The Lancet* **376**, 2104–2113 (2010).
51. Kemenesi, G. & Bányai, K. Tick-Borne Flaviviruses, with a Focus on Powassan Virus. *Clinical Microbiology Reviews* **32**, 10.1128/cmr.00106-17 (2018).
52. Dobler, G., Gniel, D., Petermann, R. & Pfeffer, M. Epidemiology and distribution of tick-borne encephalitis. *Wien Med Wochenschr* **162**, 230–238 (2012).
53. Zeng, Z., Zhan, J., Chen, L., Chen, H. & Cheng, S. Global, regional, and national dengue burden from 1990 to 2017: A systematic analysis based on the global burden of disease study 2017. *eClinicalMedicine* **32**, (2021).
54. Gaythorpe, K. A. *et al.* The global burden of yellow fever. *eLife* **10**, e64670.
55. CDC - DPDx - Ticks. <https://www.cdc.gov/dpdx/ticks/index.html> (2019).
56. Heuverswyn, J. V. *et al.* Spatiotemporal spread of tick-borne encephalitis in the EU/EEA, 2012 to 2020. *Eurosurveillance* **28**, 2200543 (2023).
57. Bakonyi, T. & Haussig, J. M. West Nile virus keeps on moving up in Europe. *Euro Surveill* **25**, 2001938 (2020).
58. Surveillance Atlas of Infectious Diseases. <https://atlas.ecdc.europa.eu/public/index.aspx?Dataset=27&HealthTopic=60>.
59. Weissenböck, H., Bakonyi, T., Rossi, G., Mani, P. & Nowotny, N. Usutu Virus, Italy, 1996. *Emerg Infect Dis* **19**, 274–277 (2013).
60. Vázquez, A. *et al.* Usutu virus – potential risk of human disease in Europe. *Eurosurveillance* **16**, 19935 (2011).



61. *Aedes albopictus* - current known distribution: February 2023. <https://www.ecdc.europa.eu/en/publications-data/aedes-albopictus-current-known-distribution-february-2023> (2023).
62. Blagrove, M. S. C. *et al.* Potential for Zika virus transmission by mosquitoes in temperate climates. *Proceedings of the Royal Society B: Biological Sciences* **287**, 20200119 (2020).
63. Gjenero-Margan, I. *et al.* Autochthonous dengue fever in Croatia, August-September 2010. *Euro Surveill* **16**, 19805 (2011).
64. La Ruche, G. *et al.* First two autochthonous dengue virus infections in metropolitan France, September 2010. *Euro Surveill* **15**, 19676 (2010).
65. Marchand, E. *et al.* Autochthonous case of dengue in France, October 2013. *Euro Surveill* **18**, 20661 (2013).
66. Sousa, C. A. *et al.* Ongoing outbreak of dengue type 1 in the Autonomous Region of Madeira, Portugal: preliminary report. *Euro Surveill* **17**, 20333 (2012).
67. Lazzarini, L. *et al.* First autochthonous dengue outbreak in Italy, August 2020. *Euro Surveill* **25**, 2001606 (2020).
68. *Culex pipiens* group - current known distribution: March 2022. <https://www.ecdc.europa.eu/en/publications-data/culex-pipiens-group-current-known-distribution-march-2022> (2022).
69. Ravanini, P. *et al.* Japanese encephalitis virus RNA detected in *Culex pipiens* mosquitoes in Italy. *Eurosurveillance* **17**, 20221 (2012).
70. Platonov, A. E. *et al.* Does the Japanese encephalitis virus (JEV) represent a threat for human health in Europe? Detection of JEV RNA sequences in birds collected in Italy. *Eurosurveillance* **17**, 20241 (2012).
71. Dick, G. W. A., Kitchen, S. F. & Haddow, A. J. Zika Virus (II). Pathogenicity and physical Properties. *Transactions of the Royal Society of Tropical Medicine and Hygiene* **46**, (1952).
72. Macnamara, F. N. Zika virus: a report on three cases of human infection during an epidemic of jaundice in Nigeria. *Trans R Soc Trop Med Hyg* **48**, 139–145 (1954).
73. Marchette, N. J., Garcia, R. & Rudnick, A. Isolation of Zika Virus from *Aedes Aegypti* Mosquitoes in Malaysia. *The American Journal of Tropical Medicine and Hygiene* **18**, 411–415 (1969).
74. Smithburn, K. C., Kerr, J. A. & Gatne, P. B. Neutralizing Antibodies Against Certain Viruses in the Sera of Residents of India. *The Journal of Immunology* **72**, 248–257 (1954).
75. Smithburn, K. C. Neutralizing antibodies against arthropod-borne viruses in the sera of long-time residents of Malaya and Borneo. *Am J Hyg* **59**, 157–163 (1954).
76. Lanciotti, R. S. *et al.* Genetic and serologic properties of Zika virus associated with an epidemic, Yap State, Micronesia, 2007. *Emerg Infect Dis* **14**, 1232–1239 (2008).

77. Haddow, A. D. *et al.* Genetic Characterization of Zika Virus Strains: Geographic Expansion of the Asian Lineage. *PLOS Neglected Tropical Diseases* **6**, e1477 (2012).
78. Olson, J. G., Ksiazek, T. G., Suhandiman, & Triwibowo. Zika virus, a cause of fever in Central Java, Indonesia. *Transactions of The Royal Society of Tropical Medicine and Hygiene* **75**, 389–393 (1981).
79. Bearcroft, W. G. Zika virus infection experimentally induced in a human volunteer. *Trans R Soc Trop Med Hyg* **50**, 442–448 (1956).
80. Filipe, A. R., Martins, C. M. V. & Rocha, H. Laboratory infection with Zika virus after vaccination against yellow fever. *Archiv f Virusforschung* **43**, 315–319 (1973).
81. Oster, A. M. Interim Guidelines for Prevention of Sexual Transmission of Zika Virus — United States, 2016. *MMWR Morb Mortal Wkly Rep* **65**, (2016).
82. Duffy, M. R. *et al.* Zika Virus Outbreak on Yap Island, Federated States of Micronesia. *N Engl J Med* **360**, 2536–2543 (2009).
83. Cao-Lormeau, V.-M. *et al.* Zika virus, French polynesia, South pacific, 2013. *Emerg Infect Dis* **20**, 1085–1086 (2014).
84. Roth, A. *et al.* Concurrent outbreaks of dengue, chikungunya and Zika virus infections – an unprecedented epidemic wave of mosquito-borne viruses in the Pacific 2012–2014. *Eurosurveillance* **19**, 20929 (2014).
85. Dupont-Rouzeyrol, M. *et al.* Co-infection with Zika and Dengue Viruses in 2 Patients, New Caledonia, 2014 - Volume 21, Number 2—February 2015 - Emerging Infectious Diseases journal - CDC. doi:10.3201/eid2102.141553.
86. Tognarelli, J. *et al.* A report on the outbreak of Zika virus on Easter Island, South Pacific, 2014. *Arch Virol* **161**, 665–668 (2016).
87. Zanoluca, C. *et al.* First report of autochthonous transmission of Zika virus in Brazil. *Mem Inst Oswaldo Cruz* **110**, 569–572 (2015).
88. Rapid risk assessment: Zika virus epidemic in the Americas: potential association with microcephaly and Guillain-Barré syndrome - 4th update, 10 December 2015. *European Centre for Disease Prevention and Control* <https://www.ecdc.europa.eu/en/publications-data/rapid-risk-assessment-zika-virus-epidemic-americas-potential-association> (2015).
89. WHO statement on the first meeting of the International Health Regulations (2005) (IHR 2005) Emergency Committee on Zika virus and observed increase in neurological disorders and neonatal malformations. [https://www.who.int/news/item/01-02-2016-who-statement-on-the-first-meeting-of-the-international-health-regulations-\(2005\)-\(ihr-2005\)-emergency-committee-on-zika-virus-and-observed-increase-in-neurological-disorders-and-neonatal-malformations](https://www.who.int/news/item/01-02-2016-who-statement-on-the-first-meeting-of-the-international-health-regulations-(2005)-(ihr-2005)-emergency-committee-on-zika-virus-and-observed-increase-in-neurological-disorders-and-neonatal-malformations).
90. McCarthy, M. Four in Florida are infected with Zika from local mosquitoes. *BMJ* **354**, i4235 (2016).

91. Zika epidemiology update - February 2022. <https://www.who.int/publications/m/item/zika-epidemiology-update---february-2022>.
92. Oehler, E. *et al.* Zika virus infection complicated by Guillain-Barré syndrome – case report, French Polynesia, December 2013. *Eurosurveillance* **19**, 20720 (2014).
93. Parra, B. *et al.* Guillain–Barré Syndrome Associated with Zika Virus Infection in Colombia. *New England Journal of Medicine* **375**, 1513–1523 (2016).
94. Brasil, P. *et al.* Guillain-Barré syndrome associated with Zika virus infection. *The Lancet* **387**, 1482 (2016).
95. Mattar, S. *et al.* Case report: microcephaly associated with Zika virus infection, Colombia. *BMC Infect Dis* **17**, 423 (2017).
96. Besnard, M. *et al.* Congenital cerebral malformations and dysfunction in fetuses and newborns following the 2013 to 2014 Zika virus epidemic in French Polynesia. *Euro Surveill* **21**, (2016).
97. Calvet, G. *et al.* Detection and sequencing of Zika virus from amniotic fluid of fetuses with microcephaly in Brazil: a case study. *The Lancet Infectious Diseases* **16**, 653–660 (2016).
98. de Noronha, L., Zanoluca, C., Azevedo, M. L. V., Luz, K. G. & dos Santos, C. N. D. Zika virus damages the human placental barrier and presents marked fetal neurotropism. *Mem Inst Oswaldo Cruz* **111**, 287–293 (2016).
99. A Socio-economic Impact Assessment of the Zika Virus in Latin America and the Caribbean | United Nations Development Programme. *UNDP* <https://www.undp.org/publications/socio-economic-impact-assessment-zika-virus-latin-america-and-caribbean>.
100. Dumpis, U., Crook, D. & Oksi, J. Tick-Borne Encephalitis. *Clin Infect Dis* **28**, 882–890 (1999).
101. Offerdahl, D. K., Clancy, N. G. & Bloom, M. E. Stability of a Tick-Borne Flavivirus in Milk. *Front Bioeng Biotechnol* **4**, 40 (2016).
102. Ecker, M., Allison, S. L., Meixner, T. & Heinz, F. X. Sequence analysis and genetic classification of tick-borne encephalitis viruses from Europe and Asia. *J Gen Virol* **80** ( Pt 1), 179–185 (1999).
103. Yoshii, K., Song, J. Y., Park, S.-B., Yang, J. & Schmitt, H.-J. Tick-borne encephalitis in Japan, Republic of Korea and China. *Emerg Microbes Infect* **6**, e82 (2017).
104. Haglund, M. & Günther, G. Tick-borne encephalitis--pathogenesis, clinical course and long-term follow-up. *Vaccine* **21 Suppl 1**, S11-18 (2003).
105. Atrasheuskaya, A. V., Fredeking, T. M. & Ignatyev, G. M. Changes in immune parameters and their correction in human cases of tick-borne encephalitis. *Clin Exp Immunol* **131**, 148–154 (2003).

106. Günther, G., Haglund, M., Lindquist, L., Sköldenberg, B. & Forsgren, M. Intrathecal IgM, IgA and IgG antibody response in tick-borne encephalitis. Long-term follow-up related to clinical course and outcome. *Clinical and Diagnostic Virology* **8**, 17–29 (1997).
107. Mickienė, A. *et al.* Tickborne Encephalitis in an Area of High Endemicity in Lithuania: Disease Severity and Long-Term Prognosis. *Clinical Infectious Diseases* **35**, 650–658 (2002).
108. Tick Borne Encephalitis (TBE) – sjukdomsstatistik. <https://www.folkhalsomyndigheten.se/folkhalsorapportering-statistik/statistik-a-o/sjukdomsstatistik/tick-borne-encephalitis-tbe/>.
109. Erbel, P. *et al.* Structural basis for the activation of flaviviral NS3 proteases from dengue and West Nile virus. *Nat Struct Mol Biol* **13**, 372–373 (2006).
110. Falgout, B., Miller, R. H. & Lai, C. J. Deletion analysis of dengue virus type 4 nonstructural protein NS2B: identification of a domain required for NS2B-NS3 protease activity. *Journal of Virology* **67**, 2034–2042 (1993).
111. Noble, C. G., Seh, C. C., Chao, A. T. & Shi, P. Y. Ligand-bound structures of the dengue virus protease reveal the active conformation. *J Virol* **86**, 438–446 (2012).
112. Palanisamy, N., Akaberi, D. & Lennerstrand, J. Protein backbone flexibility pattern is evolutionarily conserved in the Flaviviridae family: A case of NS3 protease in Flavivirus and Hepacivirus. *Mol. Phylogenet. Evol.* **118**, 58–63 (2018).
113. Akaberi, D. *et al.* Targeting the NS2B-NS3 protease of tick-borne encephalitis virus with pan-flaviviral protease inhibitors. *Antiviral Research* **190**, 105074 (2021).
114. Chappell, K. J., Stoermer, M. J., Fairlie, D. P. & Young, P. R. Insights to Substrate Binding and Processing by West Nile Virus NS3 Protease through Combined Modeling, Protease Mutagenesis, and Kinetic Studies\*. *Journal of Biological Chemistry* **281**, 38448–38458 (2006).
115. Pettersen, E. F. *et al.* UCSF Chimera--a visualization system for exploratory research and analysis. *J Comput Chem* **25**, 1605–1612 (2004).
116. Zhang, Z. *et al.* Crystal structure of unlinked NS2B-NS3 protease from Zika virus. *Science* **354**, 1597–1600 (2016).
117. Biochemical characterisation of Murray Valley encephalitis virus proteinase. *FEBS Letters* **584**, 3149–3152 (2010).
118. Junaid, M. *et al.* Enzymatic Analysis of Recombinant Japanese Encephalitis Virus NS2B(H)-NS3pro Protease with Fluorogenic Model Peptide Substrates. *PLOS ONE* **7**, e36872 (2012).
119. Bessaud, M. *et al.* Identification and enzymatic characterization of NS2B-NS3 protease of Alkhurma virus, a class-4 flavivirus. *Virus Research* **107**, 57–62 (2005).

120. Nall, T. A. *et al.* Enzymatic Characterization and Homology Model of a Catalytically Active Recombinant West Nile Virus NS3 Protease \*. *Journal of Biological Chemistry* **279**, 48535–48542 (2004).
121. Leung, D. *et al.* Activity of Recombinant Dengue 2 Virus NS3 Protease in the Presence of a Truncated NS2B Co-factor, Small Peptide Substrates, and Inhibitors \*. *Journal of Biological Chemistry* **276**, 45762–45771 (2001).
122. Phoo, W. W. *et al.* Structure of the NS2B-NS3 protease from Zika virus after self-cleavage. *Nature Communications* **7**, 13410 (2016).
123. Kondo, M. Y. *et al.* Yellow fever virus NS2B/NS3 protease: Hydrolytic Properties and Substrate Specificity. *Biochemical and Biophysical Research Communications* **407**, 640–644 (2011).
124. Behnam, M. A. M., Graf, D., Bartenschlager, R., Zlotos, D. P. & Klein, C. D. Discovery of Nanomolar Dengue and West Nile Virus Protease Inhibitors Containing a 4-Benzyloxyphenylglycine Residue. *J. Med. Chem.* **58**, 9354–9370 (2015).
125. Weigel, L. F., Nitsche, C., Graf, D., Bartenschlager, R. & Klein, C. D. Phenylalanine and Phenylglycine Analogues as Arginine Mimetics in Dengue Protease Inhibitors. *J. Med. Chem.* **58**, 7719–7733 (2015).
126. Nitsche, C. *et al.* Peptide–Boronic Acid Inhibitors of Flaviviral Proteases: Medicinal Chemistry and Structural Biology. *J. Med. Chem.* **60**, 511–516 (2017).
127. Marsault, E. & Peterson, M. L. Macrocycles Are Great Cycles: Applications, Opportunities, and Challenges of Synthetic Macrocycles in Drug Discovery. *J. Med. Chem.* **54**, 1961–2004 (2011).
128. Braun, N. J. *et al.* Structure-Based Macrocyclization of Substrate Analogue NS2B-NS3 Protease Inhibitors of Zika, West Nile and Dengue viruses. *ChemMedChem* **15**, 1439–1452 (2020).
129. Huber, S. *et al.* Structure-Based Optimization and Characterization of Macrocyclic Zika Virus NS2B-NS3 Protease Inhibitors. *J. Med. Chem.* **65**, 6555–6572 (2022).
130. Köhl, N. *et al.* A New Class of Dengue and West Nile Virus Protease Inhibitors with Submicromolar Activity in Reporter Gene DENV-2 Protease and Viral Replication Assays. *J. Med. Chem.* **63**, 8179–8197 (2020).
131. Köhl, N., Leuthold, M. M., Behnam, M. A. M. & Klein, C. D. Beyond Basicity: Discovery of Nonbasic DENV-2 Protease Inhibitors with Potent Activity in Cell Culture. *J. Med. Chem.* **64**, 4567–4587 (2021).
132. Gorbalenya, A. E. *et al.* The species Severe acute respiratory syndrome-related coronavirus: classifying 2019-nCoV and naming it SARS-CoV-2. *Nat Microbiol* **5**, 536–544 (2020).
133. El-Sayed, A. & Kamel, M. Coronaviruses in humans and animals: the role of bats in viral evolution. *Environ Sci Pollut Res* **28**, 19589–19600 (2021).

134. Laue, M. *et al.* Morphometry of SARS-CoV and SARS-CoV-2 particles in ultrathin plastic sections of infected Vero cell cultures. *Sci Rep* **11**, 3515 (2021).
135. Wu, A. *et al.* Genome Composition and Divergence of the Novel Coronavirus (2019-nCoV) Originating in China. *Cell Host & Microbe* **27**, 325–328 (2020).
136. Grellet, E., L'Hôte, I., Goulet, A. & Imbert, I. Replication of the coronavirus genome: A paradox among positive-strand RNA viruses. *Journal of Biological Chemistry* **298**, (2022).
137. Hoffmann, M. *et al.* SARS-CoV-2 Cell Entry Depends on ACE2 and TMPRSS2 and Is Blocked by a Clinically Proven Protease Inhibitor. *Cell* **181**, 271–280.e8 (2020).
138. Bosch, B. J., van der Zee, R., de Haan, C. A. M. & Rottier, P. J. M. The Coronavirus Spike Protein Is a Class I Virus Fusion Protein: Structural and Functional Characterization of the Fusion Core Complex. *Journal of Virology* **77**, 8801–8811 (2003).
139. Belouzard, S., Chu, V. C. & Whittaker, G. R. Activation of the SARS coronavirus spike protein via sequential proteolytic cleavage at two distinct sites. *Proc Natl Acad Sci U S A* **106**, 5871–5876 (2009).
140. Hoffmann, M., Kleine-Weber, H. & Pöhlmann, S. A Multibasic Cleavage Site in the Spike Protein of SARS-CoV-2 Is Essential for Infection of Human Lung Cells. *Molecular Cell* **78**, 779–784.e5 (2020).
141. Mondal, T., Shivange, G., Habieb, A. & Tushir-Singh, J. A Feasible Alternative Strategy Targeting Furin Disrupts SARS-CoV-2 Infection Cycle. *Microbiology Spectrum* **10**, e02364-21 (2022).
142. Shang, J. *et al.* Cell entry mechanisms of SARS-CoV-2. *Proc Natl Acad Sci U S A* **117**, 11727–11734 (2020).
143. Peacock, T. P. *et al.* The furin cleavage site in the SARS-CoV-2 spike protein is required for transmission in ferrets. *Nat Microbiol* **6**, 899–909 (2021).
144. Tang, T. *et al.* Proteolytic Activation of SARS-CoV-2 Spike at the S1/S2 Boundary: Potential Role of Proteases beyond Furin. *ACS Infect. Dis.* **7**, 264–272 (2021).
145. Bj, B., W, B. & Pj, R. Cathepsin L functionally cleaves the severe acute respiratory syndrome coronavirus class I fusion protein upstream of rather than adjacent to the fusion peptide. *Journal of virology* **82**, (2008).
146. V'kovski, P., Kratzel, A., Steiner, S., Stalder, H. & Thiel, V. Coronavirus biology and replication: implications for SARS-CoV-2. *Nat Rev Microbiol* **19**, 155–170 (2021).
147. Angelini, M. M., Akhlaghpour, M., Neuman, B. W. & Buchmeier, M. J. Severe Acute Respiratory Syndrome Coronavirus Nonstructural Proteins 3, 4, and 6 Induce Double-Membrane Vesicles. *mBio* **4**, 10.1128/mbio.00524-13 (2013).

148. Oudshoorn, D. *et al.* Expression and Cleavage of Middle East Respiratory Syndrome Coronavirus nsp3-4 Polypeptide Induce the Formation of Double-Membrane Vesicles That Mimic Those Associated with Coronavirus RNA Replication. *mBio* **8**, 10.1128/mbio.01658-17 (2017).
149. Klein, S. *et al.* SARS-CoV-2 structure and replication characterized by in situ cryo-electron tomography. *Nat Commun* **11**, 5885 (2020).
150. Knoops, K. *et al.* SARS-Coronavirus Replication Is Supported by a Reticulovesicular Network of Modified Endoplasmic Reticulum. *PLOS Biology* **6**, e226 (2008).
151. Malone, B., Urakova, N., Snijder, E. J. & Campbell, E. A. Structures and functions of coronavirus replication-transcription complexes and their relevance for SARS-CoV-2 drug design. *Nat Rev Mol Cell Biol* **23**, 21–39 (2022).
152. Wolff, G. *et al.* A molecular pore spans the double membrane of the coronavirus replication organelle. *Science* **369**, 1395–1398 (2020).
153. Prydz, K. & Saraste, J. The life cycle and enigmatic egress of coronaviruses. *Molecular Microbiology* **117**, 1308–1316 (2022).
154. Lu, S. *et al.* The SARS-CoV-2 nucleocapsid phosphoprotein forms mutually exclusive condensates with RNA and the membrane-associated M protein. *Nat Commun* **12**, 502 (2021).
155. Ghosh, S. *et al.*  $\beta$ -Coronaviruses Use Lysosomes for Egress Instead of the Biosynthetic Secretory Pathway. *Cell* **183**, 1520–1535.e14 (2020).
156. Chen, D. *et al.* ORF3a of SARS-CoV-2 promotes lysosomal exocytosis-mediated viral egress. *Developmental Cell* **56**, 3250–3263.e5 (2021).
157. Tan, W. *et al.* A Novel Coronavirus Genome Identified in a Cluster of Pneumonia Cases — Wuhan, China 2019–2020. *CCDCW* **2**, 61–62 (2020).
158. Zhu, N. *et al.* A Novel Coronavirus from Patients with Pneumonia in China, 2019. *N Engl J Med* **382**, 727–733 (2020).
159. CDC. Healthcare Workers. *Centers for Disease Control and Prevention* <https://www.cdc.gov/coronavirus/2019-ncov/hcp/clinical-care/clinical-considerations-presentation.html> (2020).
160. Huang, C. *et al.* Clinical features of patients infected with 2019 novel coronavirus in Wuhan, China. *The Lancet* **395**, 497–506 (2020).
161. Wang, D. *et al.* Clinical Characteristics of 138 Hospitalized Patients With 2019 Novel Coronavirus-Infected Pneumonia in Wuhan, China. *JAMA* **323**, 1061–1069 (2020).
162. Lamers, M. M. & Haagmans, B. L. SARS-CoV-2 pathogenesis. *Nat Rev Microbiol* **20**, 270–284 (2022).
163. Viana, R. *et al.* Rapid epidemic expansion of the SARS-CoV-2 Omicron variant in southern Africa. *Nature* **603**, 679–686 (2022).

164. Galmiche, S. *et al.* SARS-CoV-2 incubation period across variants of concern, individual factors, and circumstances of infection in France: a case series analysis from the ComCor study. *The Lancet Microbe* **4**, e409–e417 (2023).
165. Hyams, C. *et al.* Severity of Omicron (B.1.1.529) and Delta (B.1.617.2) SARS-CoV-2 infection among hospitalised adults: a prospective cohort study in Bristol, United Kingdom. *The Lancet Regional Health – Europe* **25**, (2023).
166. Abdullah, F. *et al.* Decreased severity of disease during the first global omicron variant covid-19 outbreak in a large hospital in tshwane, south africa. *International Journal of Infectious Diseases* **116**, 38–42 (2022).
167. Menni, C. *et al.* Symptom prevalence, duration, and risk of hospital admission in individuals infected with SARS-CoV-2 during periods of omicron and delta variant dominance: a prospective observational study from the ZOE COVID Study. *The Lancet* **399**, 1618–1624 (2022).
168. Hui, K. P. Y. *et al.* SARS-CoV-2 Omicron variant replication in human bronchus and lung ex vivo. *Nature* **603**, 715–720 (2022).
169. Willett, B. J. *et al.* SARS-CoV-2 Omicron is an immune escape variant with an altered cell entry pathway. *Nat Microbiol* **7**, 1161–1179 (2022).
170. Li, C. *et al.* Human airway and nasal organoids reveal escalating replicative fitness of SARS-CoV-2 emerging variants. *Proceedings of the National Academy of Sciences* **120**, e2300376120 (2023).
171. Hui, K. P. Y. *et al.* Replication of SARS-CoV-2 Omicron BA.2 variant in ex vivo cultures of the human upper and lower respiratory tract. *EBioMedicine* **83**, 104232 (2022).
172. Zhang, L. *et al.* Crystal structure of SARS-CoV-2 main protease provides a basis for design of improved  $\alpha$ -ketoamide inhibitors. *Science* **368**, 409–412 (2020).
173. Osipiuk, J. *et al.* Structure of papain-like protease from SARS-CoV-2 and its complexes with non-covalent inhibitors. *Nat Commun* **12**, 743 (2021).
174. Ullrich, S. & Nitsche, C. The SARS-CoV-2 main protease as drug target. *Bioorg Med Chem Lett* **30**, 127377 (2020).
175. Zhang, L. *et al.*  $\alpha$ -Ketoamides as Broad-Spectrum Inhibitors of Coronavirus and Enterovirus Replication: Structure-Based Design, Synthesis, and Activity Assessment. *J Med Chem* **63**, 4562–4578 (2020).
176. Lutten, A. *et al.* Ultralarge Virtual Screening Identifies SARS-CoV-2 Main Protease Inhibitors with Broad-Spectrum Activity against Coronaviruses. *J. Am. Chem. Soc.* **144**, 2905–2920 (2022).
177. Owen, D. R. *et al.* An oral SARS-CoV-2 Mpro inhibitor clinical candidate for the treatment of COVID-19. *Science* **374**, 1586–1593 (2021).
178. Unoh, Y. *et al.* Discovery of S-217622, a Noncovalent Oral SARS-CoV-2 3CL Protease Inhibitor Clinical Candidate for Treating COVID-19. *J. Med. Chem.* **65**, 6499–6512 (2022).



179. Adjei, S. Mortality Risk Among Patients Hospitalized Primarily for COVID-19 During the Omicron and Delta Variant Pandemic Periods — United States, April 2020–June 2022. *MMWR Morb Mortal Wkly Rep* **71**, (2022).
180. Ward, I. L. *et al.* Risk of covid-19 related deaths for SARS-CoV-2 omicron (B.1.1.529) compared with delta (B.1.617.2): retrospective cohort study. *BMJ* **378**, e070695 (2022).
181. Kurhade, C. *et al.* Low neutralization of SARS-CoV-2 Omicron BA.2.75.2, BQ.1.1 and XBB.1 by parental mRNA vaccine or a BA.5 bivalent booster. *Nat Med* 1–4 (2022) doi:10.1038/s41591-022-02162-x.
182. Lyke, K. E. *et al.* Rapid decline in vaccine-boosted neutralizing antibodies against SARS-CoV-2 Omicron variant. *Cell Reports Medicine* **3**, 100679 (2022).
183. Wang, Q. *et al.* Alarming antibody evasion properties of rising SARS-CoV-2 BQ and XBB subvariants. *Cell* **0**, (2022).
184. Andrews, N. *et al.* Covid-19 Vaccine Effectiveness against the Omicron (B.1.1.529) Variant. *New England Journal of Medicine* **386**, 1532–1546 (2022).
185. Hammond, J. *et al.* Oral Nirmatrelvir for High-Risk, Nonhospitalized Adults with Covid-19. *N Engl J Med* **386**, 1397–1408 (2022).
186. Shionogi, press release. Xocova® (Emsitrelvir Fumaric Acid) Tablets 125mg Approved in Japan for the Treatment of SARS-CoV-2 Infection, under the Emergency Regulatory Approval System. <https://www.shionogi.com/us/en/news/2022/11/xocova-ensitrelvir-fumaric-acid-tablets-125mg-approved-in-japan-for-the-treatment-of-sars-cov-2-infection,-under-the-emergency-regulatory-approval-system.html> (2022).
187. Rawlings, N. D., Barrett, A. J. & Finn, R. Twenty years of the MEROPS database of proteolytic enzymes, their substrates and inhibitors. *Nucleic Acids Res* **44**, D343-350 (2016).
188. Kim, S. *et al.* PubChem Substance and Compound databases. *Nucleic Acids Res* **44**, D1202-1213 (2016).
189. Hsu, K.-C., Chen, Y.-F., Lin, S.-R. & Yang, J.-M. iGEMDOCK: a graphical environment of enhancing GEMDOCK using pharmacological interactions and post-screening analysis. *BMC Bioinformatics* **12 Suppl 1**, S33 (2011).
190. Trott, O. & Olson, A. J. AutoDock Vina: improving the speed and accuracy of docking with a new scoring function, efficient optimization and multithreading. *J Comput Chem* **31**, 455–461 (2010).
191. Sandeep, G., Nagasree, K. P., Hanisha, M. & Kumar, M. M. K. AU-Docker LE: A GUI for virtual screening with AUTODOCK Vina. *BMC Res Notes* **4**, 445 (2011).
192. Lei, J. *et al.* Crystal structure of Zika virus NS2B-NS3 protease in complex with a boronate inhibitor. *Science* **353**, 503–505 (2016).

193. Akaberi, D. *et al.* Baseline dasabuvir resistance in Hepatitis C virus from the genotypes 1, 2 and 3 and modeling of the NS5B-dasabuvir complex by the in silico approach. *Infection Ecology & Epidemiology* **8**, 1528117 (2018).
194. Hess, B., Kutzner, C., van der Spoel, D. & Lindahl, E. GROMACS 4: Algorithms for Highly Efficient, Load-Balanced, and Scalable Molecular Simulation. *J. Chem. Theory Comput.* **4**, 435–447 (2008).
195. Lindorff-Larsen, K. *et al.* Improved side-chain torsion potentials for the Amber ff99SB protein force field. *Proteins* **78**, 1950–1958 (2010).
196. Wang, J., Wolf, R. M., Caldwell, J. W., Kollman, P. A. & Case, D. A. Development and testing of a general amber force field. *Journal of Computational Chemistry* **25**, 1157–1174 (2004).
197. Bauer, P. *et al.* Q6: A comprehensive toolkit for empirical valence bond and related free energy calculations. *SoftwareX* **7**, 388–395 (2018).
198. Jorgensen, W. L., Maxwell, D. S. & Tirado-Rives, J. Development and Testing of the OPLS All-Atom Force Field on Conformational Energetics and Properties of Organic Liquids. *J. Am. Chem. Soc.* **118**, 11225–11236 (1996).
199. Hansson, T., Marelus, J. & Åqvist, J. Ligand binding affinity prediction by linear interaction energy methods. *J Comput Aided Mol Des* **12**, 27–35 (1998).
200. Hansson, T., Marelus, J. & Åqvist, J. Ligand binding affinity prediction by linear interaction energy methods. *J Comput Aided Mol Des* **12**, 27–35 (1998).
201. Almlöf, M., Carlsson, J. & Åqvist, J. Improving the Accuracy of the Linear Interaction Energy Method for Solvation Free Energies. *J. Chem. Theory Comput.* **3**, 2162–2175 (2007).
202. Nissen, K. *et al.* Presymptomatic viral shedding and infective ability of SARS-CoV-2; a case report. *Heliyon* **7**, e06328 (2021).
203. Ling, J. *et al.* Infectious SARS-CoV-2 is rarely present in the nasopharynx samples collected from Swedish hospitalized critically ill COVID-19 patients. *Ir J Med Sci* **192**, 227–229 (2023).
204. Corman, V. M. *et al.* Detection of 2019 novel coronavirus (2019-nCoV) by real-time RT-PCR. *Eurosurveillance* **25**, 2000045 (2020).
205. Houston, D. R. & Walkinshaw, M. D. Consensus Docking: Improving the Reliability of Docking in a Virtual Screening Context. *J. Chem. Inf. Model.* **53**, 384–390 (2013).
206. Pyring, D. *et al.* Design and Synthesis of Potent C2-Symmetric Diol-Based HIV-1 Protease Inhibitors: Effects of Fluoro Substitution. *J. Med. Chem.* **44**, 3083–3091 (2001).
207. Lv, Z., Chu, Y. & Wang, Y. HIV protease inhibitors: a review of molecular selectivity and toxicity. *HIV* **7**, 95–104 (2015).
208. Li, Y. *et al.* Structural Dynamics of Zika Virus NS2B-NS3 Protease Binding to Dipeptide Inhibitors. *Structure* **25**, 1242-1250.e3 (2017).

209. Jaenson, T. G. T., Hjertqvist, M., Bergström, T. & Lundkvist, A. Why is tick-borne encephalitis increasing? A review of the key factors causing the increasing incidence of human TBE in Sweden. *Parasit Vectors* **5**, 184 (2012).
210. Li, J. *et al.* Functional Profiling of Recombinant NS3 Proteases from All Four Serotypes of Dengue Virus Using Tetrapeptide and Octapeptide Substrate Libraries \*. *Journal of Biological Chemistry* **280**, 28766–28774 (2005).
211. Cregar-Hernandez, L. *et al.* Small Molecule Pan-Dengue and West Nile Virus NS3 Protease Inhibitors. *Antivir Chem Chemother* **21**, 209–217 (2011).
212. Raut, R. *et al.* A small molecule inhibitor of dengue virus type 2 protease inhibits the replication of all four dengue virus serotypes in cell culture. *Virology Journal* **12**, 16 (2015).
213. Wu, H. *et al.* Novel Dengue Virus NS2B/NS3 Protease Inhibitors. *Antimicrobial Agents and Chemotherapy* **59**, 1100–1109 (2015).
214. Asghar, N. *et al.* Tick-Borne Encephalitis Virus Sequenced Directly from Questing and Blood-Feeding Ticks Reveals Quasispecies Variance. *PLoS One* **9**, (2014).
215. Sali, A. & Blundell, T. L. Comparative protein modelling by satisfaction of spatial restraints. *J Mol Biol* **234**, 779–815 (1993).
216. Akaberi, D. *et al.* Identification of a C2-symmetric diol based human immunodeficiency virus protease inhibitor targeting Zika virus NS2B-NS3 protease. *Journal of Biomolecular Structure and Dynamics* **0**, 1–11 (2019).
217. Kuiper, B. D. *et al.* Increased activity of unlinked Zika virus NS2B/NS3 protease compared to linked Zika virus protease. *Biochemical and Biophysical Research Communications* **492**, 668–673 (2017).
218. Sarkar, S. *et al.* DelPhi Web Server: A Comprehensive Online Suite for Electrostatic Calculations of Biological Macromolecules and Their Complexes. *Communications in Computational Physics* **13**, 269–284 (2013).
219. Kurz, M., Stefan, N., Zhu, J. & Skern, T. NS2B/3 proteolysis at the C-prM junction of the tick-borne encephalitis virus polyprotein is highly membrane dependent. *Virus Res* **168**, 48–55 (2012).
220. Kim, Y. M. *et al.* NMR Analysis of a Novel Enzymatically Active Unlinked Dengue NS2B-NS3 Protease Complex. *J Biol Chem* **288**, 12891–12900 (2013).
221. Keyaerts, E. *et al.* Inhibition of SARS-coronavirus infection in vitro by S-nitroso-N-acetylpenicillamine, a nitric oxide donor compound. *Int. J. Infect. Dis.* **8**, 223–226 (2004).
222. Åkerström, S. *et al.* Nitric Oxide Inhibits the Replication Cycle of Severe Acute Respiratory Syndrome Coronavirus. *Journal of Virology* **79**, 1966–1969 (2005).

- 223. Saura, M. *et al.* An Antiviral Mechanism of Nitric Oxide: Inhibition of a Viral Protease. *Immunity* **10**, 21–28 (1999).
- 224. Clark, M. A. *et al.* Design, synthesis and selection of DNA-encoded small-molecule libraries. *Nat Chem Biol* **5**, 647–654 (2009).
- 225. Lan, S. *et al.* Nirmatrelvir Resistance in SARS-CoV-2 Omicron\_BA.1 and WA1 Replicons and Escape Strategies. 2022.12.31.522389 Preprint at <https://doi.org/10.1101/2022.12.31.522389> (2023).
- 226. Zhou, Y. *et al.* Nirmatrelvir-resistant SARS-CoV-2 variants with high fitness in an infectious cell culture system. *Science Advances* **8**, eadd7197 (2022).
- 227. Boras, B. *et al.* Preclinical characterization of an intravenous coronavirus 3CL protease inhibitor for the potential treatment of COVID19. *Nat Commun* **12**, 6055 (2021).
- 228. Hoffman, R. L. *et al.* Discovery of Ketone-Based Covalent Inhibitors of Coronavirus 3CL Proteases for the Potential Therapeutic Treatment of COVID-19. *J. Med. Chem.* **63**, 12725–12747 (2020).



# Acta Universitatis Upsaliensis

*Digital Comprehensive Summaries of Uppsala Dissertations from the Faculty of Medicine 1968*

Editor: The Dean of the Faculty of Medicine

A doctoral dissertation from the Faculty of Medicine, Uppsala University, is usually a summary of a number of papers. A few copies of the complete dissertation are kept at major Swedish research libraries, while the summary alone is distributed internationally through the series Digital Comprehensive Summaries of Uppsala Dissertations from the Faculty of Medicine. (Prior to January, 2005, the series was published under the title "Comprehensive Summaries of Uppsala Dissertations from the Faculty of Medicine".)



Distribution: [publications.uu.se](http://publications.uu.se)  
urn:nbn:se:uu:diva-508907

ACTA UNIVERSITATIS  
UPSALIENSIS  
2023